Advances in Steam Path Technology

John I. Cofer, IV
John K. Reinker
William J. Sumner
GE Power Systems
Schenectady, NY

GE Power Generation

Advances in Steam Path Technology

John I. Cofer, IV
John K. Reinker
William J. Sumner
GE Power Systems
Schenectady, NY

John I. Cofer, IV

Jack began his career at GE in 1974 as a marine turbine requisition and development engineer in the Medium Steam Turbine Department in Lynn, MA. In 1979 he received the GE Power Systems Sector Engineering Award for Young Engineer in the Industrial and Marine Steam Turbine Division.

For the past 18 years, he has provided technical leadership in the development and use of advanced numerical and analytical methods for the design of turbomachinery, with special emphasis on aerodynamics, fluid mechanics and numerical optimization.

Jack has held several management positions in which he was responsible for the development of new, advanced aerodynamic designs for steam turbines for Navy surface ship and submarine propulsion, for commercial power generation, and for mechanical-drive applications.

He is Manager of Aerodynamics Engineering. He is responsible for leading a team of engineers in the development of new high-efficiency turbine and exhaust hood design concepts. .

He holds a BSAE from the University of Virginia, an MS in aeronautics and astronautics from the Massachusetts Institute of Technology, and an ME degree from Northeastern University.

John K. Reinker

John joined GE's Power Generation Business in 1984 as a Steam Turbine Engineer. He has worked in several design offices culminating in his assignment of Manager New Unit Design for Small and Large Steam Turbines. He was named to his current position of Product Line Leader - Large Steam Turbine in June 1996.

William J. Sumner

Bill is a Senior Engineer in GE's Steam Turbine Design and Development Engineering Department. He is currently working in the Steam Turbine Advance Design Department.

Since joining GE in 1971, Bill has been responsible for both experimental and analytical emission, moisture erosion, flow measurement, and solid particle erosion.

Bill has co-authored numerous technical papers and twice received the ASME-EEI Prime Mover Award. He has three patents.

A list of figures and tables appears at the end of this paper

ADVANCES IN STEAM PATH TECHNOLOGY

J.I. Cofer, IV, J.K. Reinker and W.J. Sumner
GE Power Systems
Schenectady, NY

ABSTRACT

For many years, GE has been conducting research to better understand the loss mechanisms that degrade the aerodynamic performance of steam turbine stages, and to develop new computational fluid dynamics (CFD) computer programs to predict these losses accurately. This paper describes a number of new steam path design features introduced to the GE steam turbine product line to improve turbine performance and reliability. These features include diaphragms with contoured sidewalls; Advanced Vortex blading with compound tangential lean, new continuously-coupled last-stage buckets with improved aerodynamic efficiency and reliability, improved downward and axial flow exhaust hoods; and better steam leakage control devices. The benefits of these new features for new units and retrofits of existing units are discussed.

In addition, this paper discusses the new generation of three dimensional viscous CFD analysis codes being used to develop new design concepts, including codes developed by GE as well as those obtained externally. Also described are the extensive laboratory test programs being conducted to validate the CFD codes and verify the predicted efficiency gains for new design features.

Lastly, new and unique state-of-the-art steam path design automation and optimization tools that have been developed by GE to dramatically reduce the design cycle time for new advanced aerodynamic designs are discussed.

INTRODUCTION

Turbine Efficiency Losses

The thermodynamic performance of a steam power plant depends on many factors, including cycle arrangement and inlet and exhaust steam conditions. However, the dominant contributor to the overall power plant efficiency is the steam turbine itself. The thermodynamic and aerodynamic performance of the steam turbine is primarily determined by steam path components, including the valves, inlet, nozzles, buckets, steam leakage control devices and the exhaust. To maximize power plant efficiency, aerodynamic and steam leakage losses in the turbine steam path must be minimized in both the rotating and stationary components. Figure 1 shows the types of efficiency losses that occur in a typical turbine stage and the approximate percentage that each type contributes to the total stage loss. Nozzle and bucket aerodynamic profile losses, secondary flow losses, and leakage losses account for roughly 80% to 90% of the total stage losses.

Nozzle and bucket profile losses can be significant if the blade shapes are not optimized for the local operating conditions. Profile losses are driven by surface finish, total blade surface area, airfoil shape and surface velocity distributions, and proper matching between nozzle and buckets to minimize incidence losses.

Equally significant losses can be caused by the complex secondary flows (Figure 2, adapted from Reference 1) generated as the viscous boundary layers along the inner and outer sidewalls of the steam path are turned through the blade rows. These complex, three dimension flows must be thoroughly understood before effective methods can be developed to reduce the associated losses.

Steam leakage through the seals between stationary and rotating components of the turbine

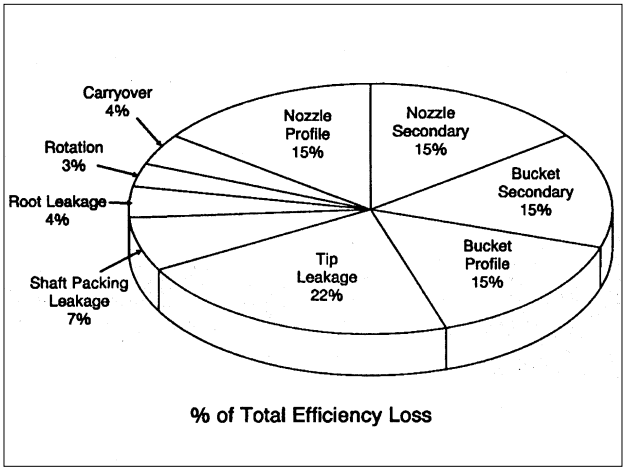

GT19893A

Figure 1. Typical HP turbine stage efficiency losses

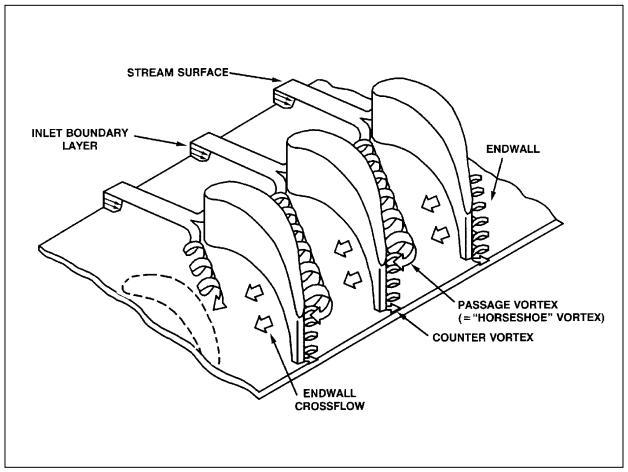

GT19894A

Figure 2. Secondary flows in a turbine nozzle cascade

constitutes an efficiency loss because the leakage flow does not contribute to the work output of the stage. This loss can be quite significant, particularly at bucket tips. In short high pressure (HP) stages, the tip leakage loss is driven by the high-stage pressure levels and the relatively larger amount of radial clearance area compared to the nozzle flow area. In taller intermediate (IP) and low pressure (LP) stages, the tip leakage loss is driven by the higher reaction levels at the bucket tips, which increases the pressure drop across the bucket tip. Steam leakage through the diaphragm shaft packing and shaft end packing also causes losses, but these are generally of lesser magnitude than tip leakage losses.

Equal attention must be paid to the losses in stationary flow path components, such as inlets, valves, and exhausts. Any pressure drop occurring in these components constitutes a loss in available energy and a reduction in work output.

Key Elements of GE Aerodynamic Development Programs

Development efforts have been underway at GE for many years to better understand and reduce the various losses listed above. The objective of this long term program is to develop specific design features, for both new turbines and retrofits of existing units, that maximize overall turbine efficiency while maintaining a high degree of reliability and cost effectiveness. Most aspects of this multifaceted development program are being conducted in cooperation with other company components, such as Aircraft Engines, Gas Turbine and Corporate Research and Development (CRD).

The four key elements of GE's overall aerodynamic development program are:

- Development of better computational fluid dynamics computer programs, which allow more accurate predictions of the complex behavior of the steam flow in the turbine
- Development of new design concepts to improve both baseline and sustained efficiency, making full use of the new CFD codes
- An extensive laboratory test program to validate the CFD codes and verify the predicted efficiency gains
- Development of a suite of powerful design automation and optimization tools to allow implementation of advanced aerodynamic design features on a custom basis to maximize efficiency for each specific application in short design cycle times

This paper reviews recent advances in GE steam path technology resulting from these development initiatives and the impact of these advances on current GE steam turbine designs.

CFD METHODS

In order to fully utilize the available energy of the steam for maximum efficiency, the complex three dimensional flow field throughout the turbine must be accurately predicted. In particular, a better understanding is needed of the effects of wet steam, viscosity, and unsteady rotor-stator interactions if the remaining losses are to be reduced. Recent advances in the development of CFD computer programs have provided GE with the tools needed to achieve better designs with reduced cost and shorter design cycle time.

Viscous Euler CFD Code

In the early 1980s, the GE steam turbine, gas turbine and aircraft engine businesses began a long-term joint research program with CRD to study secondary flow phenomena using a combined analytical and experimental approach. Analytical investigations included the development of complex computational fluid dynamics computer codes based on three dimensional formulations of the inviscid Euler equations and the viscous Navier-Stokes equations. The initial inviscid code was developed by CRD and called the EULER3D program (Reference 2). A viscous code that included turbulence models was later developed by GE Aircraft Engines and called the Viscous Euler program (References 3 and 4).

Comprehensive experimental investigations were conducted to test the validity of the predictions made by the EULER3D code. These tests

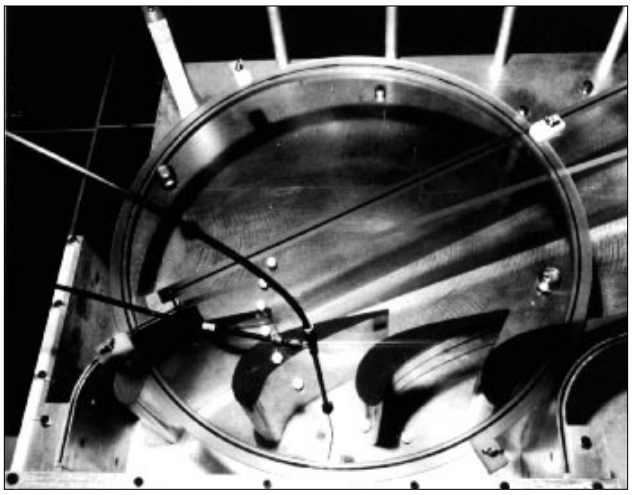

GT19895A

Figure 3. Nozzle cascade wind tunnel

utilized CRD's large-scale wind tunnel test facility (Figure 3), and the results are described in detail in Reference 5. In this study, EULER3D predictions of the flow in a subsonic turbine nozzle cascade were compared to cascade test data, including lampblack and oil flow visualization studies. Comparisons were made for nozzles with both parallel and diverging sidewalls, and the code was able to predict inviscid flows in turbine blade passages quite well.

A unique flow visualization method was developed for the wind tunnel facility to aid in understanding the physics of secondary flows. The flow particle trajectories shown in Figure 4 were obtained by shining a strobe light on helium-filled zero-buoyancy soap bubbles injected into the flow. Figure 4 clearly shows one leg of the

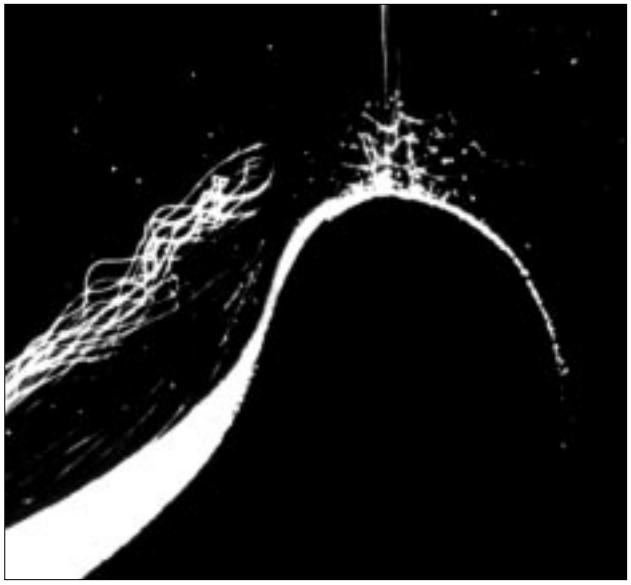

GT19897

Figure 4. Helium bubble traces in nozzle cascade

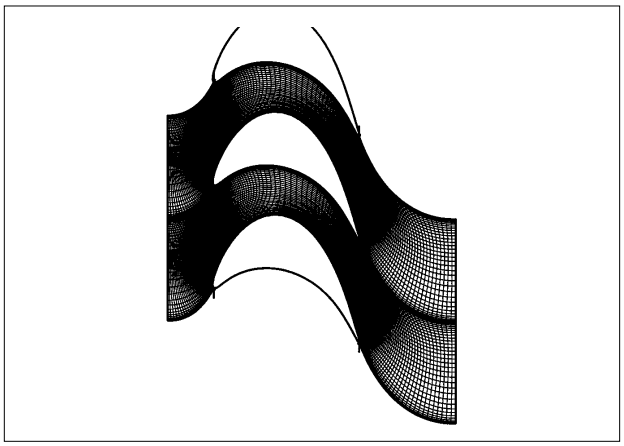

GT25784

Figure 5. HP bucket - Viscous Euler calculation grid

"horseshoe" vortex spiraling around the nose of a nozzle cascade with parallel sidewalls.

In the last few years, the Viscous Euler code has replaced EULER3D as the analysis code of choice for a wide variety of turbomachinery design problems. Improvements in computer technology have made it practical to run viscous codes such as Viscous Euler on a network of high-powered workstations, without the need for supercomputers.

Figure 5 shows the Viscous Euler calculation grid on a blade-to-blade plane for a high pressure bucket vane. A similar calculation grid is generated for the nozzle passage, and a complete stage solution is obtained by automatically iterating between the nozzle and bucket solutions as they run in parallel on separate workstations. For a complete 3D solution, up to 250,000 grid points might be needed in each blade passage to accurately resolve secondary flow details. Figure 6 shows Mach number contours for this same vane in subsonic flow, and the trailing

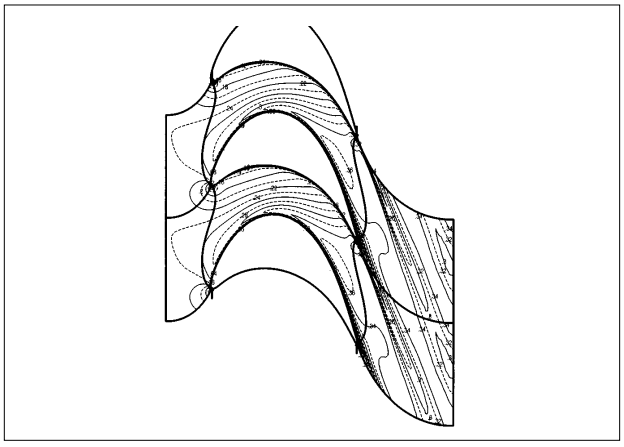

GT25785

Figure 6. HP bucket – Viscous Euler Mach number controls

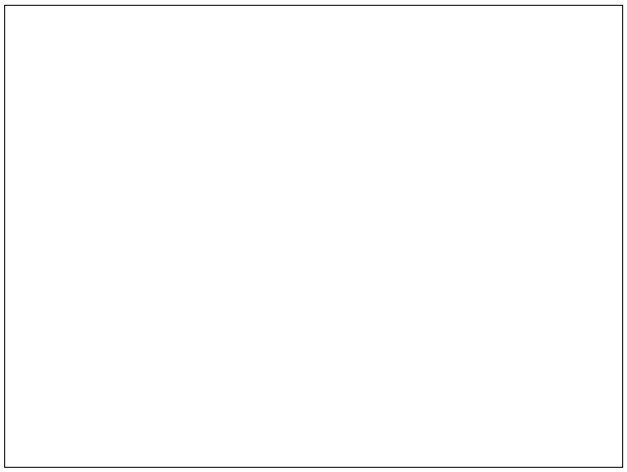

GT25993

Figure 7. IP nozzle Viscous Euler results and comparison to test data

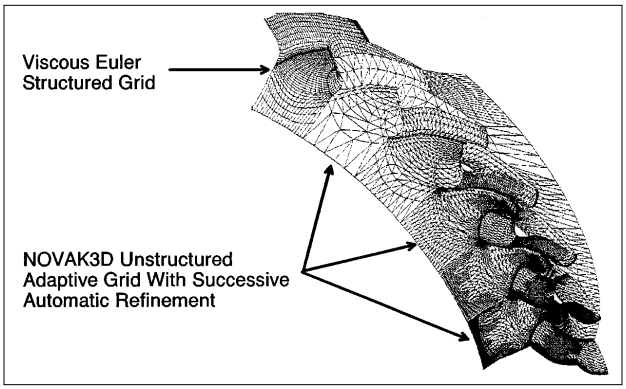

GT24583

Figure 8. Comparison of structured and unstructured grids in CFD codes.

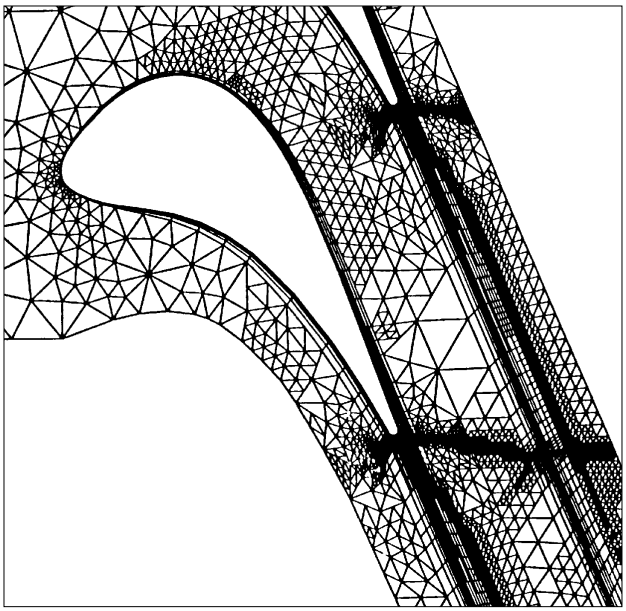

GT22182

Figure 9. NOVAK3D refined calculation grid for transonic nozzle

currently under development for incorporation into NOVAK3D. This model will include detailed 3D wet steam effects, such as homogeneous moisture droplet formation and growth, droplet trajectories and condensation shocks. The code will then be used to develop improved moisture removal devices for wet steam turbine stages. Better moisture removal devices will provide two significant benefits: improved efficiency, since stage efficiency improves about 1% for every additional 1% of moisture that is removed; and reduced bucket erosion. An extensive experimental program is planned to validate the wet steam CFD model to be incorporated in NOVAK3D.

Multi stage and Unsteady CFD Codes

A better understanding of unsteady flow effects and rotor-stator interactions is needed if the losses associated with them are to be reduced. The influence of these effects on performance has been implicitly accounted for in GE's traditional turbine performance prediction methods through the use of empirical correlations based on laboratory and field test data. However, it has been difficult to develop specific design features that reduce these losses due to the high expense and difficulty of the required testing. For this reason, renewed effort has been placed on developing the analytical capabilities to predict unsteady flows and rotor-stator interactions.

In early 1994, GE Power Generation and GE Aircraft Engines used the unsteady flow code developed by Rai and Madavan (Reference 9) to analyze a steam turbine stage with a compound lean nozzle. Because the computing time required to achieve a solution with unsteady codes is still excessive, more recent efforts have focused on the calculation of steady state multistage solutions using the passage-average approach of Adamczyk (Reference 10).

Losses due to shock waves, wakes, hub and tip leakage flows, and secondary flows propagate downstream and influence the performance of successive stages. Figure 10 shows some initial results from the Adamczyk code obtained for the third stage in a group of Advanced Vortex HP stages. The figure on the left shows vorticity contours at the nozzle exit plane, while the fig-

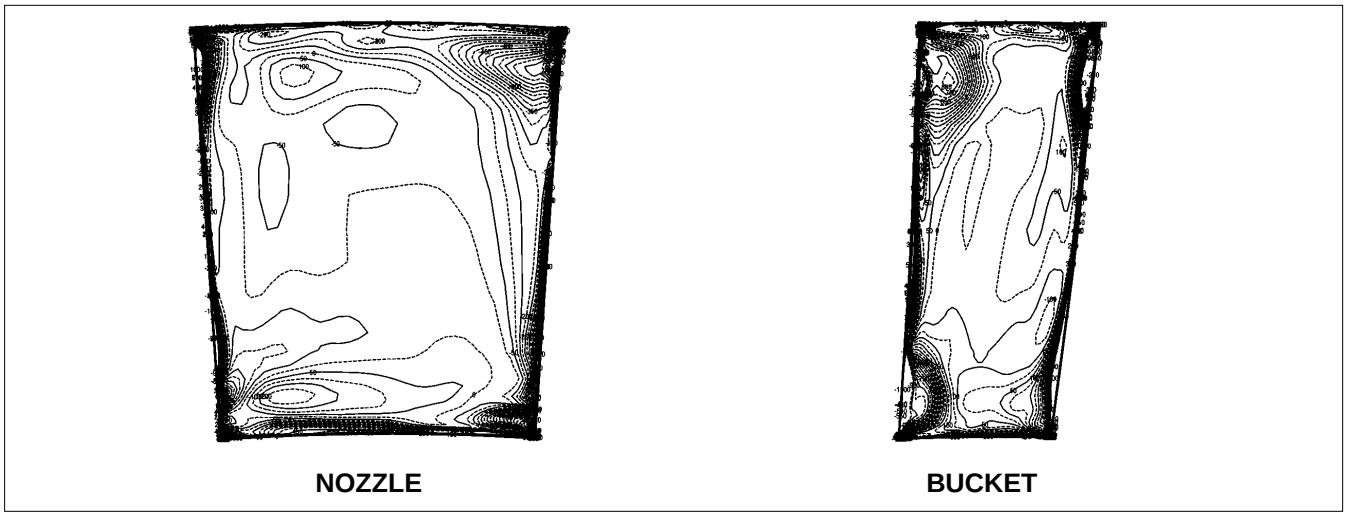

GT25787

Figure 10. Multi-stage CFD analysis — vorticity at stage 3 nozzle and bucket exit

ure on the right shows vorticity contours at the bucket exit plane. Comparisons of the code results with laboratory test data showed good agreement.

NEW DESIGN FEATURES FOR IMPROVED BASELINE EFFICIENCY

Advanced Vortex Blading

The flow inside a turbine stage must satisfy the requirements of radial equilibrium. The radial equilibrium equations are derived from the equations of motion and basic thermodynamic relations, and express the balance between pressure forces and inertial forces acting on the fluid. Before the advent of powerful computers and modern CFD codes, the complete, 3D form of these equations could not be used for practical design purposes. Designers were forced to make simplifying assumptions about the flow to reduce the radial equilibrium equations to a manageable form.

Dating back to the 1950s, GE steam turbine stages traditionally have been designed using a true free vortex radial flow distribution. In this type of design, the radial components of velocity are neglected and the assumption is made that the product of radius and tangential velocity is constant. These assumptions greatly simplify the radial equilibrium equations and result in a flow characterized by constant axial velocity and constant work at all radii in the blade row. For shorter stages, free vortex designs with tapered and twisted nozzles and buckets can be very efficient, and considerably more efficient than purely cylindrical stages. For longer stages, however, the free vortex design often results in extremely twisted buckets that are difficult to design mechanically, and it produces high tip reactions that lead to high tip leakage losses. GE has for many years designed non-free-vortex stages in LP turbines to achieve better long bucket designs.

The CFD codes available today allow accurate solutions of the fully 3D viscous Navier-Stokes flow equations, and designers are no longer bound to the free vortex concept. In 1984, GE initiated a development program to investigate various “controlled vortex” design concepts, in which the radial flow distribution is tailored to maximize the efficiency of individual stages. This program was accelerated in 1990 and expanded to include the design and testing of a number of “advanced” vortex stage designs that began with the controlled vortex concept and incorporated variable tangential lean into the nozzles. Many of these concepts have been derived from advanced GE aircraft engine design technology, and were developed jointly with GE Aircraft Engines using the Viscous Euler CFD code. An extensive ongoing test program has been underway since 1990 to verify the predicted efficiency gains for these new concepts, utilizing GE’s single-stage subsonic air turbine and the multi-stage low speed research turbine (LSRT) at GE Aircraft Engines (Figures 58 and 59, described later in this paper). All of these concepts share the following characteristics:

- The radial flow distribution is tailored to maximize efficiency based on the individual stage geometry and operating conditions
- The total nozzle surface area has been reduced relative to a conventional design by using fewer nozzles per 3608 with better aerodynamic profile shapes that retain the same total mechanical strength as a conventional design. In many cases, the number of nozzles in the diaphragm has been reduced by as much as 50%. This provides a net reduction in profile loss with no loss in mechanical integrity
- Variable tangential or compound lean is used in the nozzles when it produces a significant gain in overall stage efficiency
- Root reaction is increased in varying degrees to improve bucket root performance, and tip reaction is generally decreased relative to a free vortex design to reduce tip leakage

Due to the quite different operating conditions in HP, IP and LP stages, different concepts are used in each type of stage. In the HP section, stage pressure ratios are about 1.2. This pressure ratio is not limited by aerodynamic considerations, but rather by the pressure loading across the diaphragm at the high pressure levels occurring in the HP section. Consequently, nozzle cross-sections must be relatively larger in size than bucket cross-sections to carry the mechanical load. Figure 11 shows a typical Advanced Vortex HP stage. Figure 12 compares the radial distribution of reaction and flow angle for this design to a conventional free vortex design. In the Advanced Vortex design, overall stage reaction has been increased somewhat, although more at the root than at the tip, and root reaction is limited to about 10% to minimize thrust on the rotor. The flow angle relative to the axial

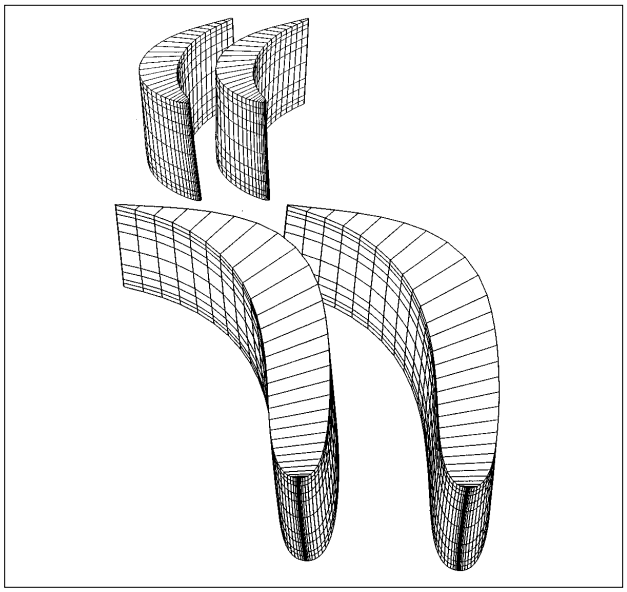

GT25788

Figure 11. Advanced Vortex HP nozzle and bucket

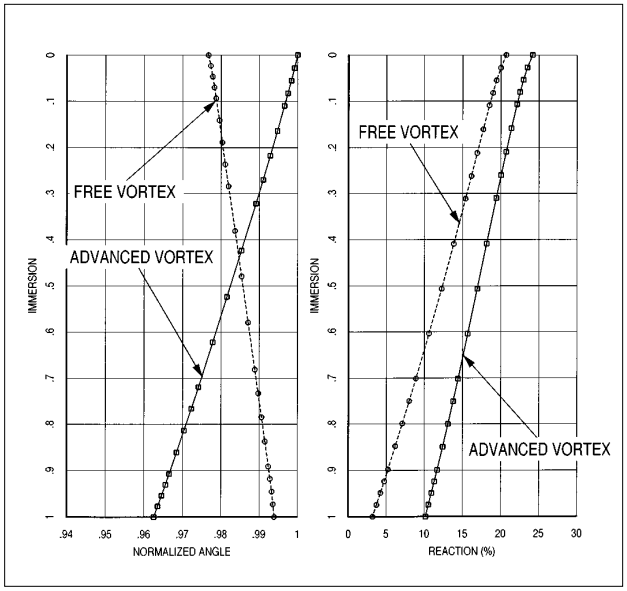

GT25789

Figure 12. HP stage nozzle exit angle and reaction distributions

direction has been decreased at the root and increased at the tip to shift flow radially inward toward the root. The flow angle shift at the root allows a more efficient, less cambered bucket root section to be designed, as shown in Figure 5. The nozzle and bucket for each stage are carefully designed as a matched set to eliminate bucket incidence angle losses. Due to the relatively low velocities in the stage (see Figure 6), the small size and strength of the secondary flow vortices, and the short blade height, nozzle lean has not proven to be an effective loss reduction method in this type of stage.

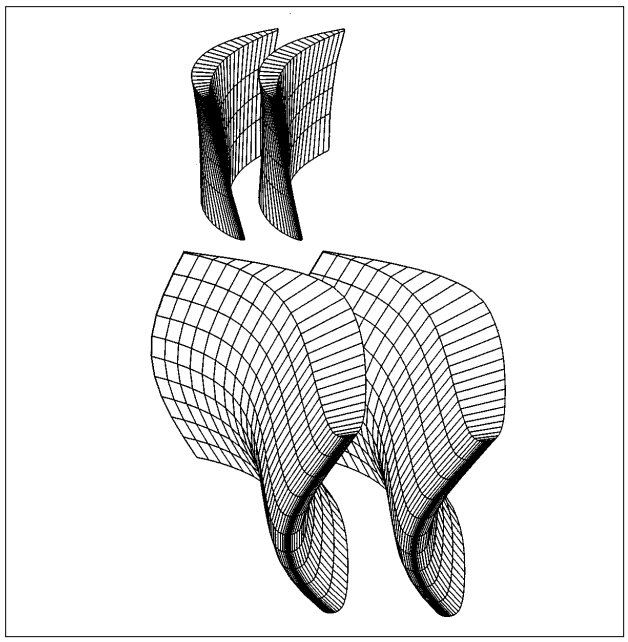

GT25790

Figure 13. Advanced Vortex IP nozzle and bucket

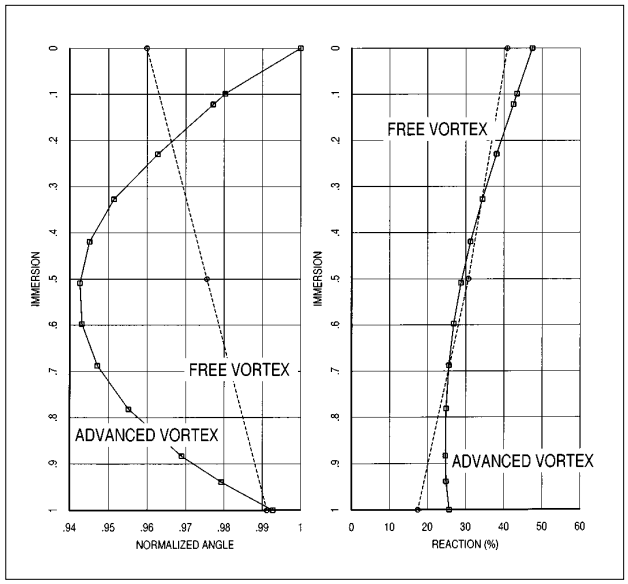

GT25791

Figure 14. IP stage nozzle exit angle and reaction distribution

In the IP section, stage pressure ratios are generally in the range of 1.2 to 1.3. Velocities are somewhat higher than in HP stages, and blades are longer and more twisted. Figure 13 shows a typical Advanced Vortex IP stage. Figure 14 compares the radial distribution of reaction and flow angle for this design to a conventional free vortex design. In these stages, the flow is biased away from the sidewalls toward the more efficient mid-section of the blade by increasing the throat at the pitchline, producing a nozzle

that is slightly overcambered at the root and tip relative to the pitchline shape. Compound lean has been introduced in the nozzle to reduce the secondary flow losses, and root reaction has been increased to allow a more efficient, less cambered bucket root section to be designed. As in the HP stage, the nozzle and bucket for each IP stage are carefully designed as a matched set to eliminate bucket incidence angle losses. The radial flow distribution in the nozzle is determined using numerical optimization techniques described later in this paper. Stage test results obtained in the subsonic air turbine have demonstrated that Advanced Vortex stages of this type are the most efficient GE has ever built.

GE's analytical studies have shown that redistributing the flow radially and leaning the nozzle have only a weak effect on overall nozzle efficiency - the losses are simply redistributed. However, if the vortexing and lean are done in the proper combination, they can reduce the size and strength of the secondary flow vortices entering the bucket, particularly at the root, which leads to substantial improvements in bucket efficiency. The nozzle and bucket must be designed as a matched set to take full advantage of the benefits of blade lean.

In the LP section, stage pressure ratios are high enough to produce transonic velocities in the last few nozzles and buckets. Buckets are long and highly twisted, and diaphragm outer sidewall slant angles can approach 508. The Advanced Vortex design concept used in the early LP stages is similar to that used in IP stages, as depicted in Figure 13.

In taller LP stages, some modifications are made to the IP design concept to produce the nozzle shown in Figure 15. First, the point of maximum bow in the blade is moved closer to the root to put more lean at the root, where it has the most benefit, and less at the tip. This also makes the blade easier to assemble in diaphragms with high outer sidewall slants. Second, a small amount of axial sweep is added to the nozzle leading edge to minimize the nozzle axial width over most of the length of the blade, thus reducing profile losses. The last-stage nozzle, and in some cases the next to the last nozzle, typically has straight tangential lean, with no bowing. In transonic nozzles, the transonic portion near the root is designed with a converging-diverging cross-section to minimize shock losses.

Each individual Advanced Vortex stage in a customer's specific application is custom-designed to optimize its efficiency in conjunction with the other stages in the turbine section. Off-the-shelf blades are seldom used, because this necessarily involves compromising the efficiency of the design to fit the existing blading. The design automation and optimization tools that allow GE to do this in a very short design cycle time are described later in this paper. Advanced Vortex nozzles and buckets are designed to meet the same strict requirements for mechanical integrity and reliability that have given GE steam turbines a record of reliability unparalleled in the industry. Concurrent with the development of new aerodynamic design concepts, modern manufacturing technologies such as five-axis NC machining, precision forging and precision casting are being utilized to allow advanced vortex blade shapes to be made with reduced cost and in shorter manufacturing cycle times.

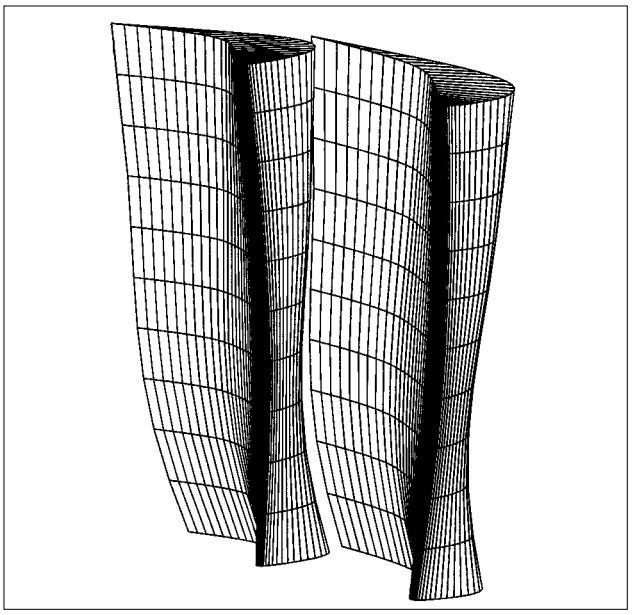

GT25792

Figure 15. Advanced Vortex LP nozzle

Overall stage efficiency gains of 2% to 2.5% have been achieved on Advanced Vortex stages relative to GE's conventional free vortex designs, which are already very efficient. This includes the combined effects of reduced nozzle count, improved profile designs, optimized radial flow distribution, nozzle lean and improved bucket tip seals. Advanced Vortex stage designs are offered as a standard feature on all new utility-type fossil reheat steam turbines rated 150 MW and above. They can also be applied to fossil reheat turbines rated below 150 MW and to combined-cycle reheat turbines, and they are available for retrofit in HP, IP and LP stages.

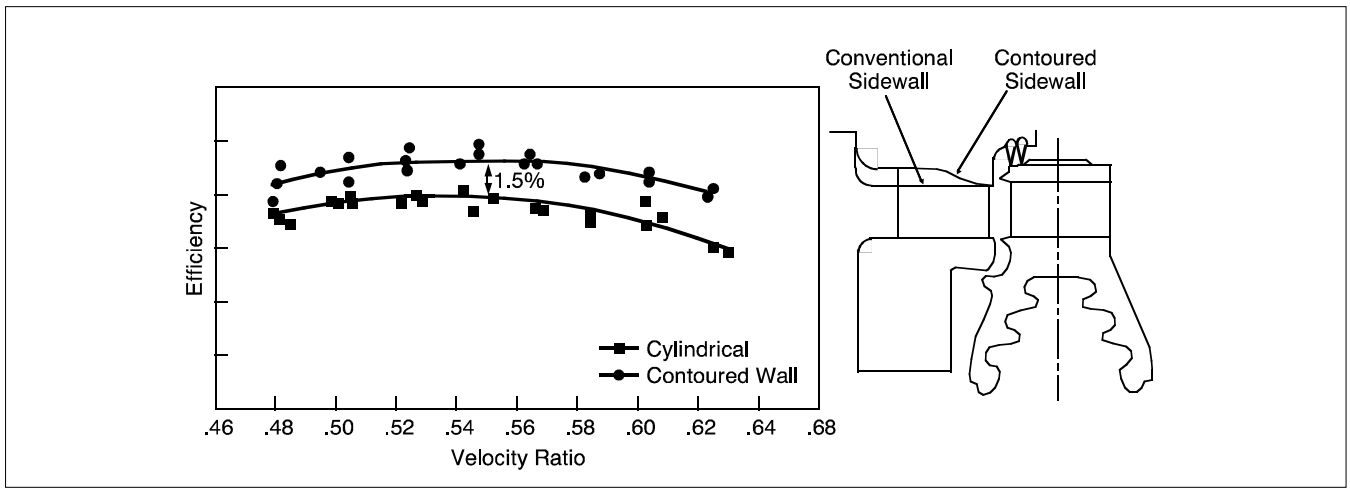

Figure 16. Contoured sidewall test data

Contoured Sidewalls

In the early 1980s, experimental investigations were conducted by CRD and the steam turbine business to determine the effects of outer sidewall contours on secondary flow losses. Prior research documented in the literature suggested that outer sidewall contours other than straight-parallel could have a beneficial effect on stage efficiency (see Reference 11). A properly designed sidewall contour reduces secondary flow losses by reducing the cross-channel pressure gradients, thereby reducing the strength of the secondary flows. The contour also reduces the size of the loss region near the inner sidewall, and reduces nozzle profile losses due to the lower velocity at nozzle inlet. Contoured sidewalls are typically used in the first stage of a turbine section.

GE's first running stage test of a steam turbine using contoured sidewalls was performed in 1983. This test was performed on a small low-energy, two-stage commercial mechanical-drive turbine that included a converging sidewall contour on the first stage and a diverging-converging contour on the second stage. The contours were designed using guidelines presented in Reference 11. An overall efficiency gain of 0.7% was realized. Wind tunnel cascade tests conducted in 1984 by CRD produced a diverging-converging sidewall contour that increased stage efficiency by 1%. An improved method for optimizing the shape of the contour for a given stage was also developed by CRD during this time period based on experimental results and extensive CFD analysis. In a parallel effort, a running stage test of a contoured sidewall was conducted in 1985 in the subsonic air turbine. The stage efficiency with the sidewall contour proved to be 1.5% greater than that for the equivalent stage with cylindrical sidewalls, as shown in Figure 16. Subsequent tests on improved contoured sidewalls yielded gains of up to 2%.

Contoured sidewalls are routinely used in mechanical-drive turbines, ships service turbine-generator sets, and in the HP, IP and LP sections of large fossil and nuclear power generation turbines, for both new units and uprate applications. A typical application might include contoured sidewalls in up to eight stages in the machine, depending on the turbine configuration, for an overall turbine efficiency gain ranging between 0.25% and 0.50% due to the contouring alone.

A family of sidewall contours has also been developed for the new solid particle erosion-resistant nozzle designs described in Reference 16. The contours improve efficiency and, at the same time, increase the resistance of the nozzle to SPE damage. These contours are available for new and retrofit nozzle box designs for control stage and first reheat stage applications.

New Last Stage Buckets

The last stage bucket is one of the most important contributors to the performance and reliability of the steam turbine. GE has developed complete families of last stage buckets (Figure 17) that provide sustained levels of high performance with virtually trouble- and maintenance-free operation. These last stage buckets all share a common continuously-coupled design technology, and they range in size from a 20-inch (508 mm) 3600 RPM bucket to a 48-inch

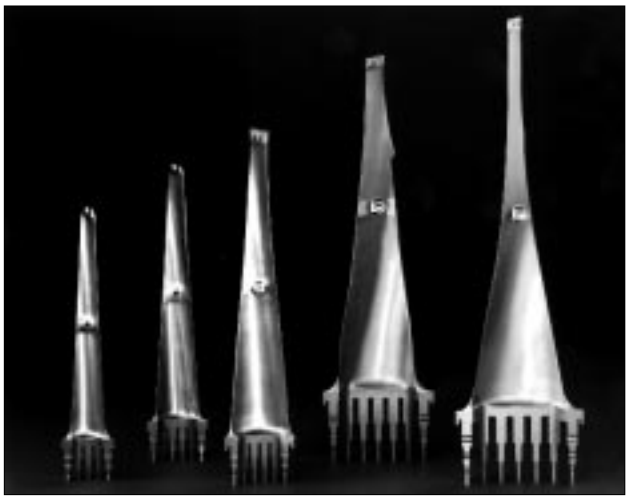

GT22198

Figure 17. 3600 rpm family of continuously coupled buckets

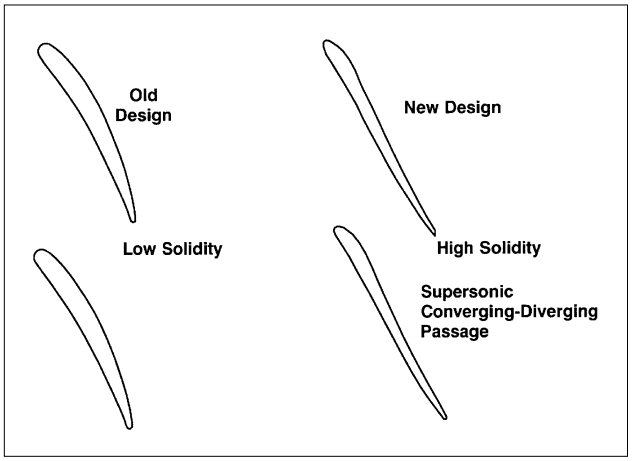

GT21881

Figure 18. Convergent-divergent supersonic bucket tip profile design

(1219 mm) 3000 RPM titanium bucket. Design features of these families include:

- Improved vane profiles, including a convergent-divergent supersonic passage design with high solidity (Figure 18)
- Improved radial mass flow distribution to optimize efficiency
- Improved tip leakage control that permits moisture removal (Figure 24)
- Continuously coupled covers, either side entry or over-and-under (Figure 19). These covers provide structural coupling and damping, and also control vane tip flow passage geometry for the reduction of leakage, secondary flow and shock losses
- Optimum location of midspan connection for structural damping and vibration control, either a loose tie wire or a nub-sleeve connection

Over/Under Cover Design of 20” (508mm) and 23” (584mm) LSB Redesign

Side Entry Cover Design of 26” (660mm) and 33.5” (851mm) LSB Redesign

GT22200A

Figure 19. Continuously coupled bucket tip design

- Self-shielded erosion protection. No separate attachment of shielding is necessary due to the use of high strength erosion-resistant materials with excellent toughness characteristics and a proven service record.

With the last stage buckets typically producing 10% of the total unit output, and up to 15% in some combined-cycle applications, improvements in last stage efficiency can significantly impact the output of the total unit. Retrofitting an older last stage design with a modern diaphragm and last stage bucket can typically improve heat rate and output by up to 1%. Typical economic payback periods for the new last stage buckets are two to three years. References 12 and 13 describe the family of modern last stage buckets in more detail. The modern buckets can be retrofit into most existing units. Table 1 lists the overall heat rate

Table 1
PERFORMANCE GAINS WITH RETROFITTED NEW LAST STAGE BUCKETS

RPM	BUCKET	OVERALL PERFORMANCE IMPROVEMENT BUCKET ONLY	BUCKET & DIAPHRAGM
3600	20 inches (508 mm)	*	0.25% ro 1.0%
	23 inches (584 mm)	0.25% to 0.75%	0.5% to 1.0%
	26 inches (660 mm)	*	1.0%
	30 inches (762 mm)	0.6%	1.0%
3000	26 inches (660 mm)	*	1.0%
1800	43 inches (1092 mm)	0.35%	0.5%

*Bucket & diaphragm replacement only

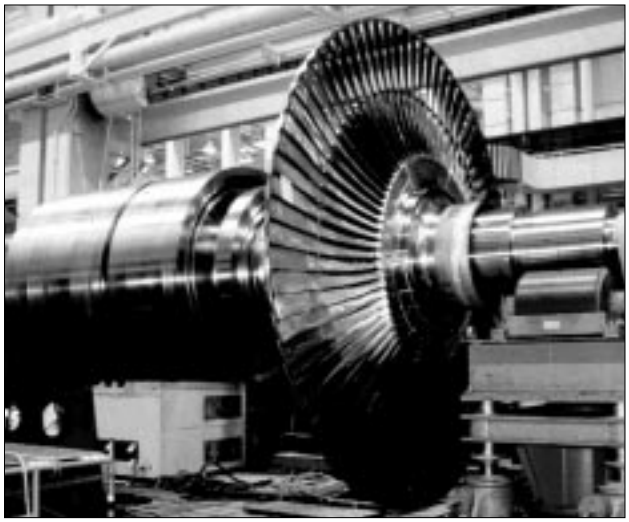

GT25793

Figure 20. 40-in. (1016 mm) titanium last stage bucket

improvements that can be expected by retrofitting the new designs in older machines.

In general, complete new modern LP turbine steam paths have been designed to go along with all of the new last stage buckets. Replacement of an older LP turbine steam path with a modern steam path design can improve heat rate by an additional 1.0% to 1.5% beyond the gain achieved by replacing the last stage alone.

In the 1960s, GE first developed the continuously coupled last stage bucket design for 3600 RPM operation with the 30-inch (762 mm) and 33.5-inch (851 mm) buckets (Reference 14). These buckets had been developed to support the increasing unit size requirements of the time and had been applied to units as large as 840 MW. With the shift of energy demands to smaller units, GE began a series of development programs to apply the latest design technology, along with the proven concepts of the 30-inch (762 mm) and 33.5-inch (851 mm) last-stage buckets, to the smaller last-stage buckets. These efforts resulted in the development of the family of modern continuously coupled last stage buckets for 3600 RPM operation shown in Figure 17. This family includes high efficiency last-stage buckets in 20-inch (508 mm), 23-inch (584 mm), 26-inch (660 mm), 30-inch (762 mm) and 33.5-inch (851 mm) sizes for both new units and the upgrade market.

A recent addition to the 3600 RPM family is a 40-inch (1016 mm) titanium last stage bucket, described in Reference 15. A series of rigorous mechanical tests of the new bucket were completed on the test rotor shown in Figure 20, and all design criteria were met. This bucket has been shipped for units in a STAG™ application. New bucket and rotor materials are being developed to allow new, even longer titanium last-stage buckets to be designed over the next several years. With longer last-stage buckets and larger annulus sizes, more compact and cost-effective turbine designs are achievable. For a more detailed discussion of GE's line of compact High-Power-Density™ turbine-generators, see Reference 16.

GE has also applied the successful continuously coupled technology to the 50-Hz product line. The new 3000 RPM last-stage buckets contain all of the modern design features listed above for the 3600 RPM family. The first of the 50-Hz product line to be modernized was the 33.5-inch (851 mm) last-stage bucket, developed in the 1980s. GE has produced several large steam turbines that utilize this bucket. Designs have also been completed that use the 33.5-inch (851 mm) last-stage bucket on combined-cycle STAG™ applications.

GT19363/GT19644

Figure 21. Comparison of single-flow 42-inch (1067 mm) and double-flow 26-inch (660 mm) units

The latest developments in the 50-Hz product line include new 26-inch (660 mm), 42-inch (1067 mm) and 48-inch (1219 mm) last-stage buckets and LP turbine steam paths. The new 26-inch (660 mm) low-pressure turbine, which is a modernization of GE's older but very successful 26-inch (660 mm) design, has been developed specifically for combined-cycle STAG™ applications. The 42-inch (1067 mm) low pressure turbine was developed to provide a more compact single-flow alternative to the double-flow 26-inch (660 mm) design for STAG™ applications. As shown in the top of Figure 21, the LP casing in the single-flow design is considerably smaller and the large crossover pipe is eliminated, compared to the double-flow design at the bottom of the figure. The 42-inch (1067 mm) last stage bucket is also used in a compact two-casing 500 MW utility unit. A 48-inch (1219 mm) titanium bucket is also available for applications requiring more annulus area.

GE continues to advance the state-of-the-art in the development of half-speed turbines for large cross-compound and nuclear units. The same advanced aerodynamic and mechanical features described above for the 3000- and 3600-RPM families have been applied to the 1500- and 1800-RPM families. These buckets have been designed with two loose tie wires, and the bucket leading edges are protected from erosion by flame hardening.

Recent developments include a 52-inch (1321 mm) 1500 RPM LP turbine for a large nuclear application. The low-pressure turbine was completely redesigned using the latest aerodynamic and mechanical design methods, resulting in improved thermodynamic performance and reliability. In addition, the 43-inch (1092 mm) last-stage bucket for 60-Hz applications has been modernized to improve its performance and reliability. Retrofitting the new bucket and diaphragm in a typical nuclear unit results in a performance improvement of 0.5%.

Bucket Tip and Shaft Packing Seals

An extended effort, until recently mostly experimental in nature, has been directed toward finding ways to minimize leakage through bucket tip and shaft packing clearances. Bucket tip leakage controls have typically utilized a single spill strip mounted on the upstream side of the bucket shroud, or two spill strips mounted on either side of the bucket cover tenon. Leakage along the shaft is controlled by packings containing multiple teeth located between the diaphragms and the shaft and at the ends of the shaft. Leakage can be reduced by either reducing the radial clearance between stationary and rotating components, or by designing the seal geometry to create a torturous path that induces turbulence and restricts the flow.

Experimental data on leakage control has been obtained largely through two-dimensional stationary air tests (such as the rig shown in Figure 57) rather than more expensive 3D rotating steam tests. Stationary air tests allow a much larger variety of leakage control configurations to be tested at relatively low cost. In the past, rotating steam tests were expensive and usually run to determine the overall effects of design changes, thus making it difficult to separate out the leakage effects. However, GE has developed a unique, cost-effective method for testing new bucket tip seal concepts in our subsonic air turbine (Figure 50), by shrink-fitting a thin ring containing the tip seal geometry onto the outer rim of the blisk test wheel (described later in this paper). By testing the wheel with and without the new seal, the effects of the seal can be isolated.

Over the years, GE has tested a great variety of bucket tip seal configurations. Figure 22 shows a sampling of these configurations. The test results show that leakage flow is substantially

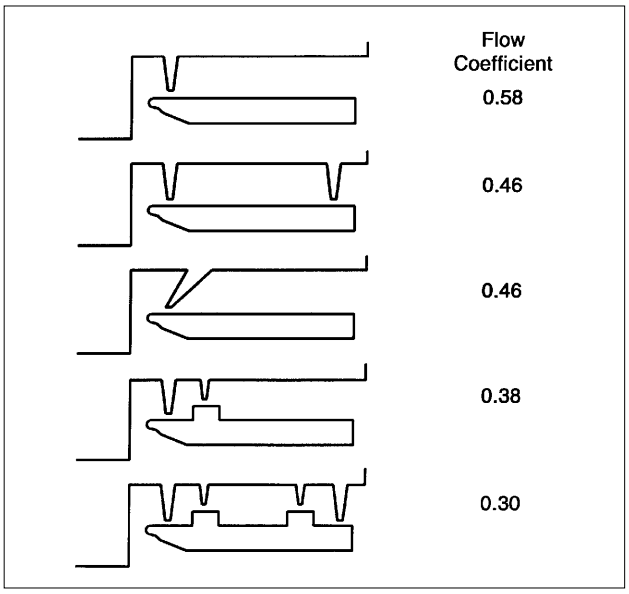

GT22123A/GT22208

Figure 22. Bucket tip leakage controls

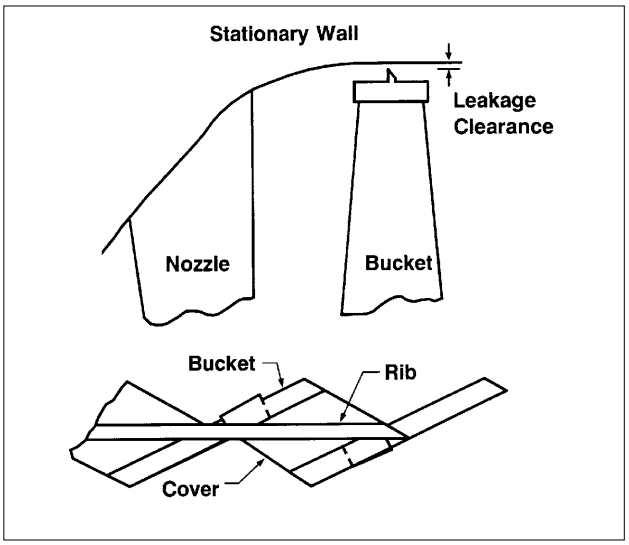

GT21884

Figure 24. Side entry last stage bucket cover design tip leakage control

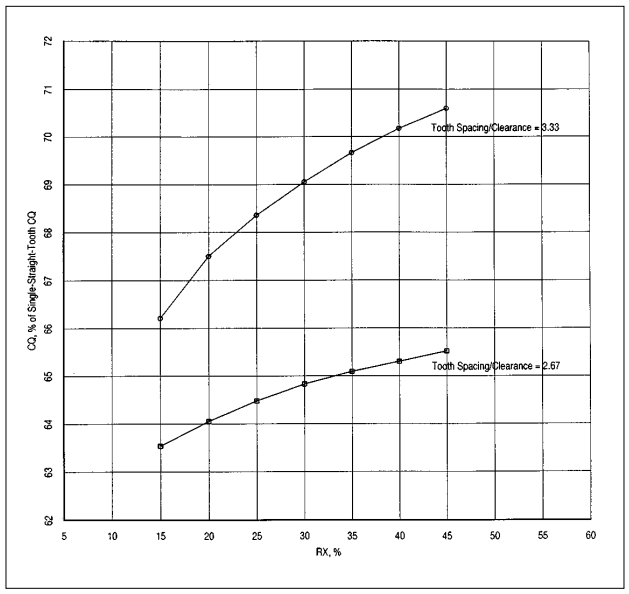

GT25794

Figure 23. Slant tooth bucket tip seal test results – optimum tooth spacing

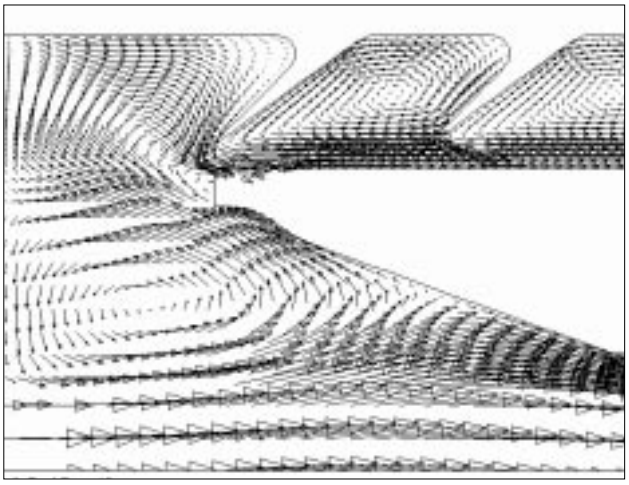

GT25798

Figure 25. CFD analysis of bucket tip seal passage – velocity vectors

reduced when a stepped or high-low spill strip is used. The configuration currently used on the majority of HP and IP bucket tip seals includes steps with double teeth on both the upstream and downstream sides of a recessed tenon. The application of these improved radial tip leakage controls improves sustained efficiency as well, because any damage to the improved controls due to a rub results in less increase in leakage than an equivalent rub to a single radial tip spill strip. Slant teeth also help to reduce leakage flow, as long as the proper tooth spacing has been selected. Figure 23 shows test data obtained in our seal test rig that illustrates the importance of choosing the optimum ratio of tooth pitch to radial clearance to minimize leakage flow.

In recent years, particular attention has been focused on last stage bucket tip leakage control. In older industrial and mechanical drive turbine designs, the only leakage control provided at the tip of the last stage bucket is the axial clearance between the downstream face of the diaphragm and the leading edge of the bucket band. This clearance generally is larger on the last stage than on any other, and the resultant leakage losses can be significant. If a radial spillband can be placed on the last-stage bucket shroud and a tight radial clearance maintained, stage efficiency can be improved by as much as 3% (depend-

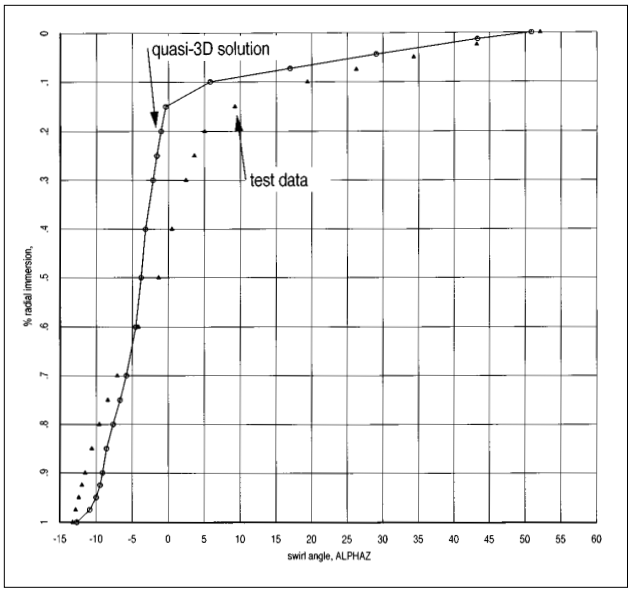

GT25795

Figure 26. Influence of tip seal re-entry flow on stage exit flow angle — comparison of quasi-3D analysis to test data

ing on bucket length), which is equivalent to about 0.3% in overall turbine efficiency. All modern GE 20-inch (508 mm) last stage buckets and larger now include a radial spillband on the bucket cover to maintain a tight radial clearance and minimize tip leakage flow. Figure 24 shows the radial spillband configuration used on the 26-inch (660 mm) and 33.5-inch (851 mm) last-stage buckets.

To complement GE's experimental program, the company is using a commercially available viscous 3D CFD code called STAR-CD to perform detailed analyses of new bucket tip leakage control and shaft packing configurations. This code has a user-friendly graphical user interface and excellent post-processing capabilities, and is ideally suited to performing parametric studies. Figure 25 shows velocity vectors calculated by STAR-CD at the leading edge of a flat bucket cover with slant teeth mounted on the casing. The code clearly shows the vortex structures in the leakage path. The code is used as a numerical test vehicle to identify promising seal configurations that warrant testing in either the stationary seal test rig or the subsonic air turbine.

A new area GE is investigating in more detail is the effect of the tip seal leakage flow on the downstream blade rows as the leakage flow reenters the steam path. The flow leaking over the top of the bucket cover enters the tip seal passage with a high tangential velocity component. While the torturous path through the seal geometry reduces the axial component of the leakage flow, it does relatively little to affect the tangential component. As the leakage flow reenters the steam path on the downstream side of the bucket, the still largely tangential flow must mix with the largely axial flow leaving the bucket. This generates mixing losses and can lead to incidence angle problems in the downstream nozzle. Traverse measurements of stage exit swirl angle obtained in the subsonic air turbine and in the low speed research turbine have confirmed this behavior, as shown in Figure 26. GE has refined the tip leakage models in its quasi-3D flow solver to reflect this behavior (also shown in Figure 26). This allows designers to more effectively account for this effect in the preliminary design of multi-stage turbines.

Exhaust Hoods

The steam leaving the last row of buckets in the turbine is directed into the condenser inlet by the exhaust casing, also known as the exhaust hood. Poor aerodynamic design of the exhaust hood can produce a large pressure drop from the last-stage bucket exit to the hood exit. This pressure drop constitutes an efficiency loss because it represents energy that cannot be used by the turbine to produce power. A well-designed hood can diffuse the flow, causing the static pressure to increase from the last stage bucket exit to the hood exit flange to match the fixed condenser pressure. This pressure recovery gives the turbine an effective back pressure that is lower than the condenser pressure, so that more energy is available for producing power. In this manner, a good diffusing hood can produce a significant overall gain in efficiency. A diffusing hood also decelerates the flow as it approaches the exhaust flange, thus reducing the likelihood of flow-generated noise and vibration in the condenser tubes.

In downward flow configurations (Figure 27), the exhaust hood must turn the flow downward 90° before it enters the condenser inlet. In the patented GE hood design concept, structural support plates inside the hood are used to partition the total flow area into smaller passages in which flow diffusion can be carefully controlled. Streamlined steam guides and flow guide vanes are used to further improve the aerodynamic performance of the flow passages so that major flow separations are avoided. Internal flanges, support struts, pipes and other protrusions into the flow passages that cause efficiency losses and generate noise are removed or minimized.

GE's approach to exhaust hood design in the

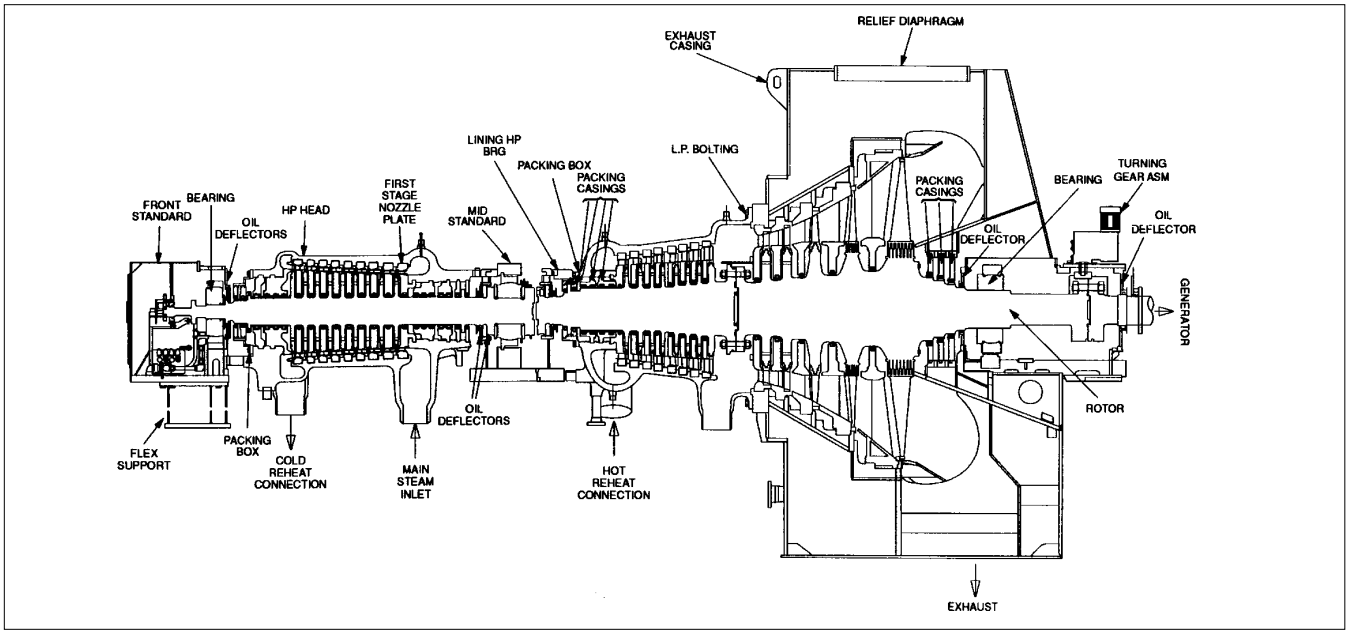

GT22194

Figure 27. Downward-flow exhaust hood

past was purely experimental. To optimize a new design, the internal flow passages of the hood were duplicated in an exact scale model (Figure 28) which was tested in an air flow test facility at GE's Aerodynamic Development Laboratory. Pressure measurements were taken at various points inside the hood model to determine the amount of flow diffusion taking place. Interchangeable parts in the model allowed many different configurations to be tested so that optimum flow passage configurations could be achieved. Since the early 1960s, literally dozens of different exhaust hood models in hundreds of different configurations have been tested, and a performance prediction and design method based on various hood geometry parameters has been developed from this extensive test data base.

Axial flow exhausts (Figure 29) have significant size and efficiency advantages over downward flow exhausts. If the requirements of the overall power plant dictate that the best location for the condenser is on the same level as the turbine exhaust, then an axial exhaust is the preferred choice. Axial flow exhausts are simpler to design and build, and can be much more efficient diffusers than downward flow exhausts because the flow does not have to be turned 90°. The velocity distribution at the exhaust flange can also be made quite uniform, resulting in improved condenser performance. Single-casing axial exhaust designs can be conveniently base-mounted for easier shipment and installation, as shown in Figure 29.

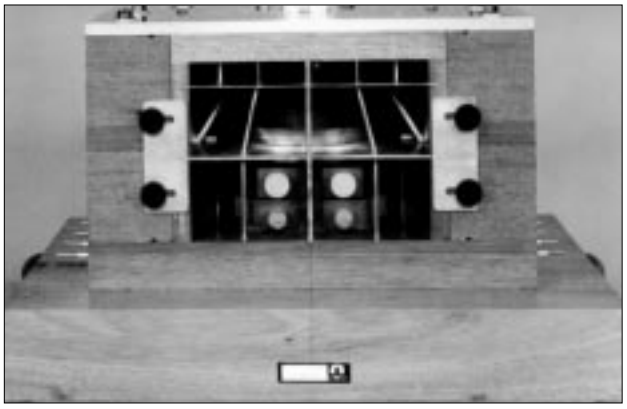

GT22195

Figure 28. Downward-flow exhaust hood test model

Axial flow hoods lend themselves to a more analytical design approach because of their simpler geometry compared to downward flow hoods. Numerous papers published in the open literature by a group of researchers at Stanford University (Kline, Johnston, et al.) have been particularly useful. However, the principal reference used as a guideline for the design of axial flow hoods is a paper by Sovran and Klomp (Reference 17). GE has designed many axial flow hoods for commercial applications based on this paper, and laboratory tests on scale models have confirmed the excellent performance of these designs.

GE's approach to exhaust hood design has improved dramatically in the last few years, with the advent of CFD codes that are capable of

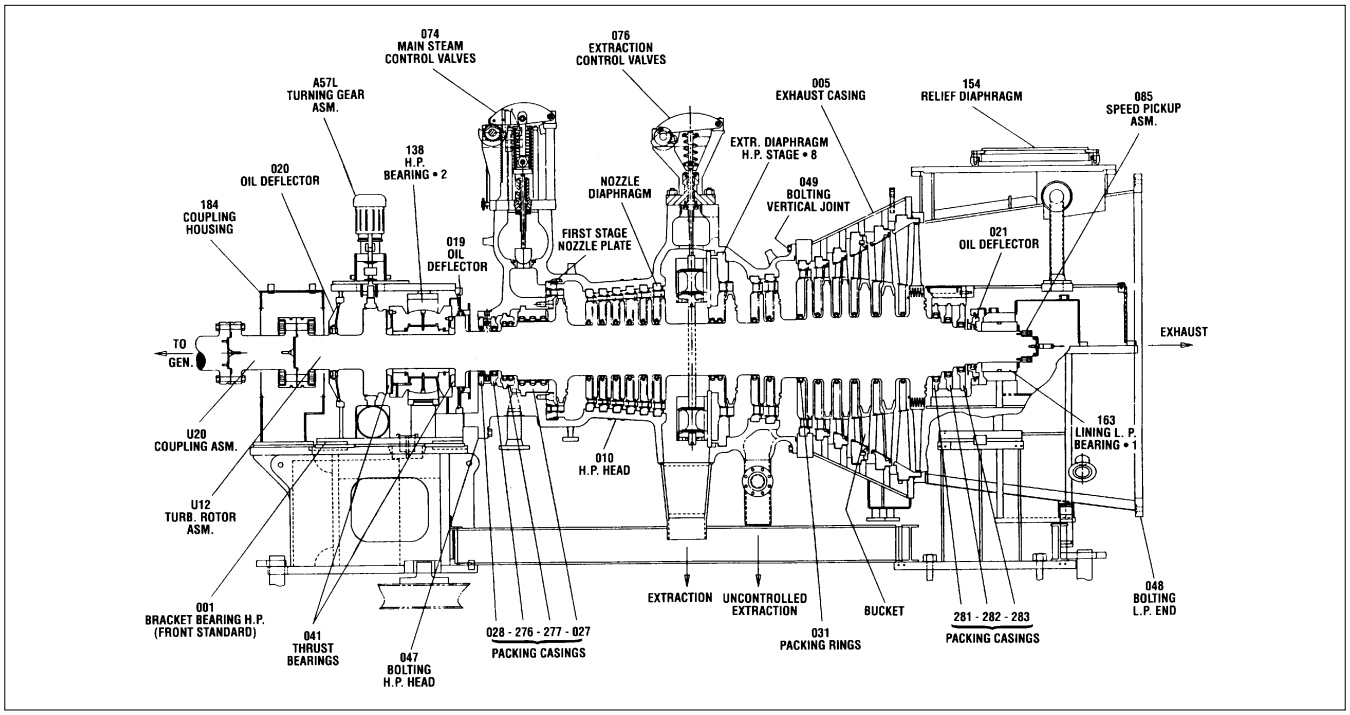

GT23020A

Figure 29. Axial-flow exhaust hood

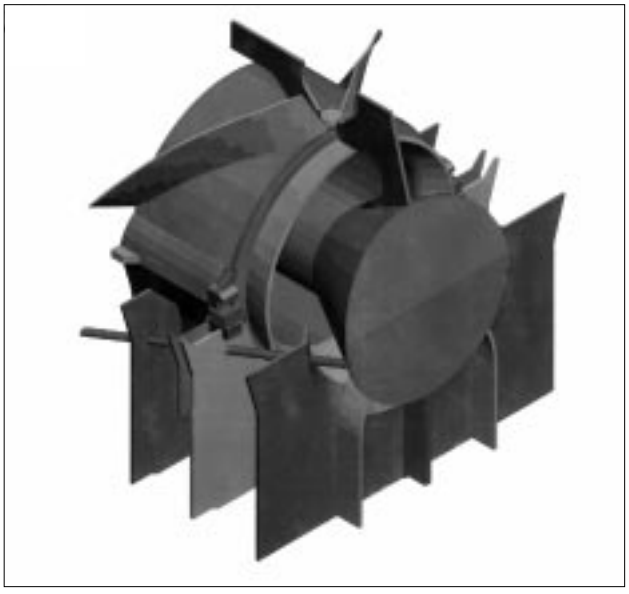

GT24590

Figure 30. Solid model of downward-flow exhaust hood for CFD analysis

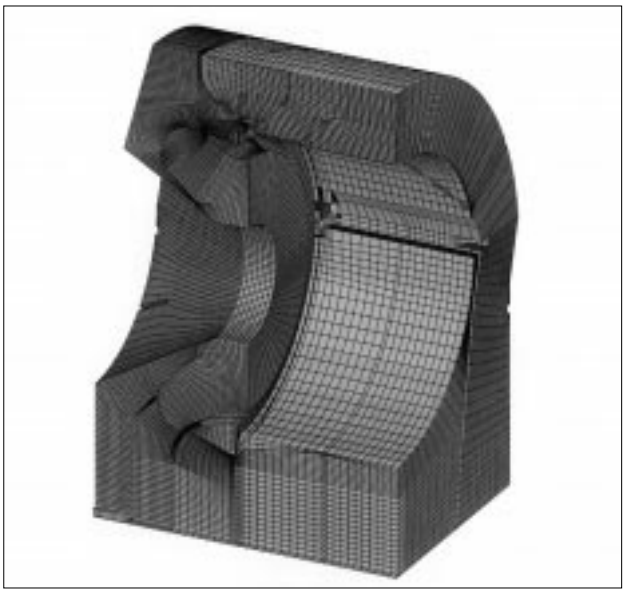

GT24591

Figure 31. Calculation grid for exhaust hood CFD analysis

accurately modeling the complex geometry and flow phenomena inside exhaust hoods. Figure 30 shows a computer-generated solid model of the internal components of a downward flow diffusing exhaust hood that had been tested in the laboratory using lampblack and oil to visualize the flow. Figure 31 shows the corresponding calculation grid required for a detailed CFD analysis of this hood. Figure 32 shows sample results from an analysis using the STAR-CD code, in this case velocity vectors and magnitudes. The code was able to predict the visualized flow features and measured pressure recovery very well. Because STAR-CD uses a structured grid approach, generating the solid model and the calculation grid took several man-months. However, this was less time than it took to build the original air test scale model, and the analysis

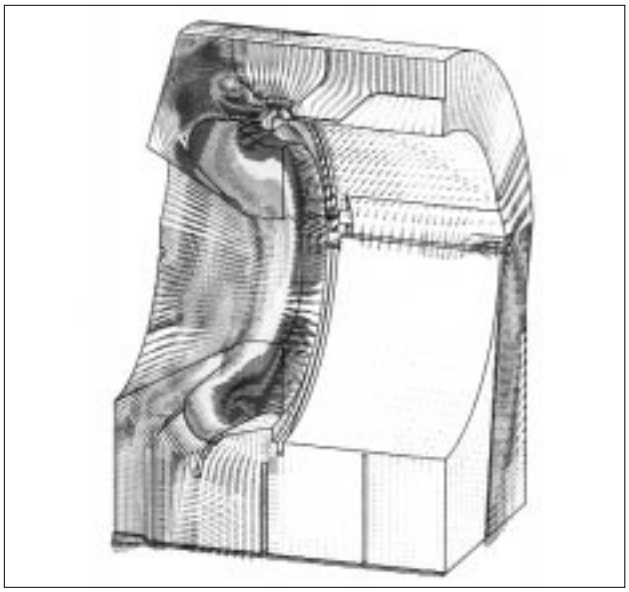

GT24592

Figure 32. Velocity vectors in downward-flow exhaust hood

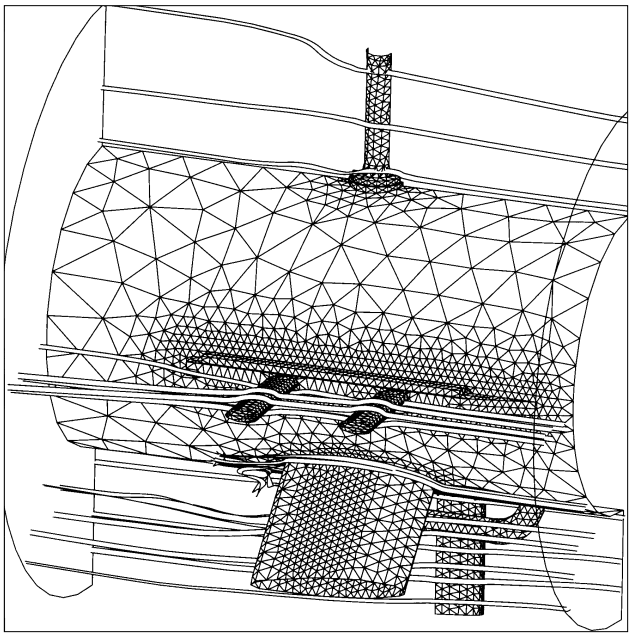

GT25796

Figure 33. NOVAK3D analysis of axial-flow exhaust with "flow ribbons"

yielded far more detailed information about the flow inside the hood than was obtained in the laboratory model tests. Numerous design refinements have already been incorporated into GE's downward flow hood designs as a result of using CFD analysis.

The NOVAK3D CFD code has proven to be an extremely useful tool for the analysis of complex stationary flow components such as exhaust hoods. Because it eliminates the need for time-consuming manual grid generation and refinement, solutions to complex problems can be obtained in a fraction of the time required with structured grid codes. Figure 33 shows an analysis of an axial flow hood that contains a number of struts, pylons and pipes. The conical outer wall has been removed for clarity, and only the surface grid is shown. Once the surface model of the hood was created using a CAD program, NOVAK3D was able to create a grid and converge to a solution in only five days on a single workstation. Figure 33 also shows "flow ribbons" that follow streamtubes through the flow, which indicate that the flow is generally well-behaved throughout the hood.

The NOVAK3D code was used to redesign the large pylons supporting the hood to eliminate large regions of separated flow downstream of the pylons. On the top portion of Figure 34, velocity vectors around the original pylon are shown. A packing seal pipe is located downstream of the pylon in a region of massive separation. On the bottom part of Figure 34, the redesigned, more streamlined pylon is shown. The packing seal pipe has been relocated inside the new pylon, and the region of separation has been eliminated.

Valves and Inlets

A new development program has been initiated to develop more efficient and cost-effective inlet and valve designs using the NOVAK3D code to analyze the flow in the complicated geometries of these components. Figures 35 through 38 show examples of the use of the code to better understand the behavior of existing valves. Figure 35 shows the surface grid generated by NOVAK3D for a steam turbine bypass valve that previously had been air tested in GE's Aerodynamic Development Laboratory. Figure 36 compares the valve flow coefficient calculated by NOVAK3D at two different valve lifts to the air test data, and it shows that NOVAK3D is able to predict the flow coefficient quite well.

Figure 37 shows the complex surface grid created by NOVAK3D for an older control valve design. This detailed model includes the holes in the strainer located in the upper part of the valve body. The "flow ribbon" plot (Figure 38) generated from the analysis of this valve shows a tightly-wound vortex structure in the lower valve body, which could be a source of pressure loss and noise generation. NOVAK3D solutions such as this have provided many valuable insights into the behavior of the flow in valves, and many improvements are being implemented to reduce valve pressure losses by up to 30%.

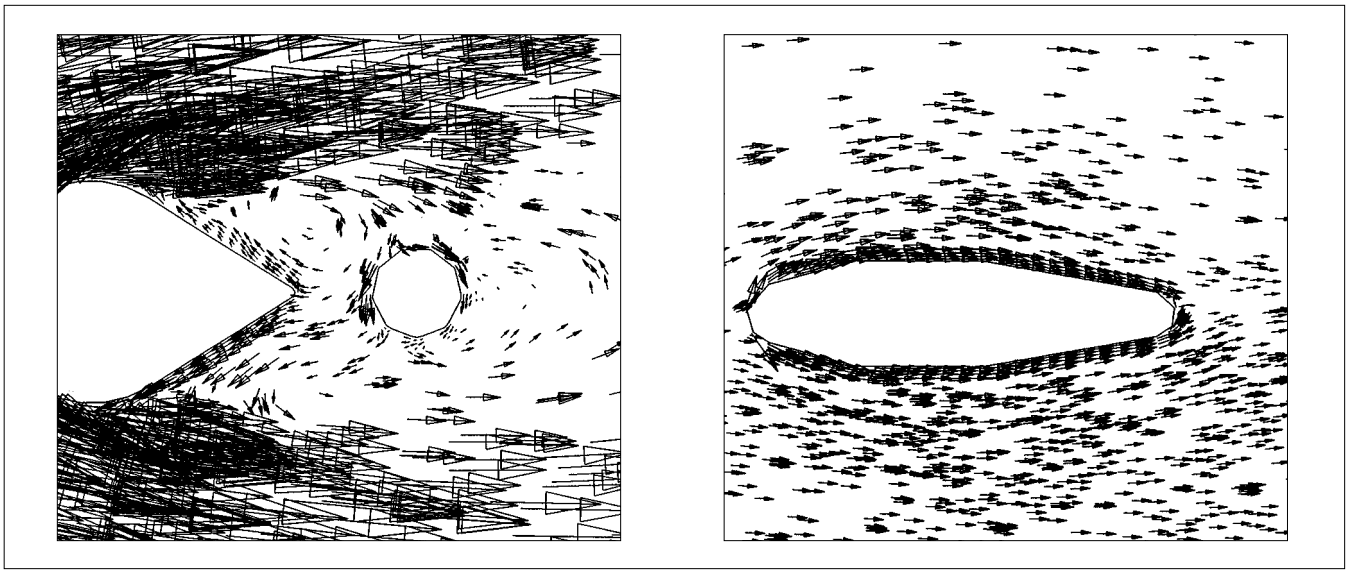

GT25797

Figure 34. NOVAK3D analysis of flow near struts in axial-flow exhaust

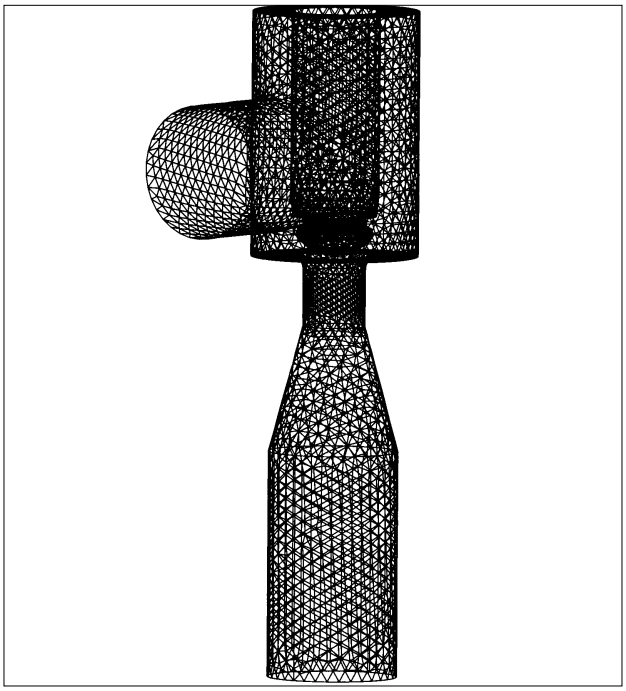

GT25803

Figure 35. NOVAK3D grid for bypass valve

NEW DESIGN FEATURES FOR IMPROVED SUSTAINED EFFICIENCY

SPE-Resistant Steam Path Designs

A primary cause of steam path efficiency degradation in units with high temperature inlet stages (> 900 F/482 C) is solid particle erosion (SPE) damage. The steam path degrades as the nozzles and buckets are worn away by the passage of steam contaminated with iron oxide particles exfoliated from the inside surfaces of boiler tubes and main and reheat steam piping. The damage results in reduced steam path efficiency, lost power generation, shortened inspection intervals and the costly repair and replacement of damaged components. Industry estimates made in the early 1980s pegged the annual industry-wide cost of SPE damage at $150 million.

In 1980, GE launched a multi-faceted development program dedicated to finding cost effective solutions to this nagging industry problem. Early in this program it was recognized that the development of a sound, fundamental understanding of the various erosion mechanisms at work in the turbine steam path would be essential to the success of any program dedicated to reducing SPE. It was further recognized that the basic elements of this understanding would have to come from analytical studies of solid particle behavior as it occurs in the steam path. The analytical capability required to accomplish this complex task was quickly put in place, becoming operational in mid-1981.

The heart of the technology is the ability to model the 3D trajectories of the particles as they pass through the steam path. This allows the identification of the locations of particle impact and the attendant critical parameters of impact velocity and impact angle which altogether define the erosion potential for a specific design. The influence of key factors such as basic stage design variables, geometry, steam conditions and mode of turbine operation can

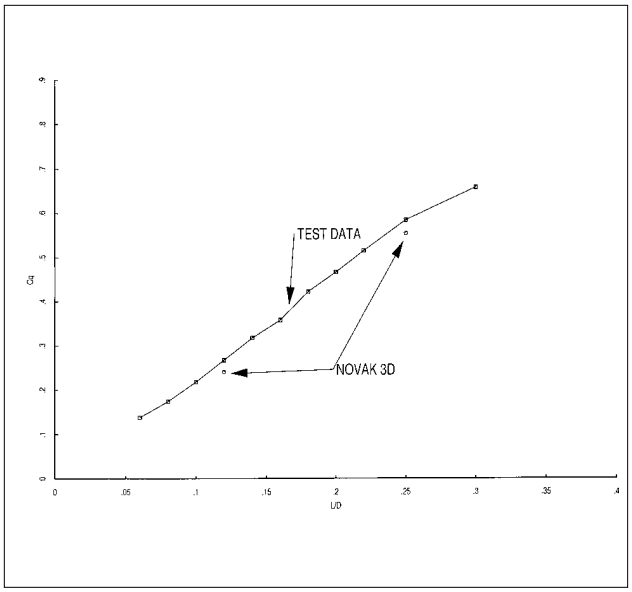

GT25799

Figure 36. NOVAK3D analysis of bypass valve – comparison of calculated flow coefficient with test data

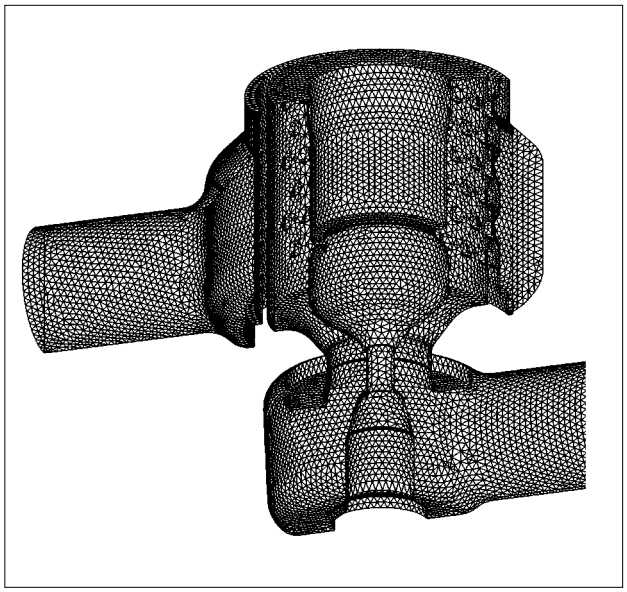

GT25804

Figure 37. NOVAK3D grid for control valve

be investigated to determine how they contribute to the occurrence of SPE damage. The ability to predict the occurrence of SPE on nozzles and buckets in HP and IP section steam paths has been clearly demonstrated with this technology. The analysis has identified the existence of completely different erosion mechanisms at work in the HP and IP turbine sections requiring different design modifications to mitigate the SPE damage.

Service experience has consistently shown that the first stage of the high pressure turbine (i.e. the control stage) and the first stage of the reheat turbine generally receive the predominant share of SPE damage in their respective sections. The following paragraphs briefly summarize the erosion mechanisms at work in these types of stages and describe field-proven design modifications that vastly reduce the susceptibility of these components to SPE damage.

Particle trajectory analysis of control stage nozzles (see Reference 18) has demonstrated that the erosion is caused by the high velocity, low angle impact of particles on the trailing edge pressure surface of the partition. The calculated range of impact angles coincides with that which produces the maximum erosion rate in nozzle partition material. One commonly used means of reducing the damage is the application of an erosion-resistant coating. The various coating alternatives available for control stage nozzle assemblies are described in detail in Reference 18. This component requires a non-line-of-sight coating process to provide protection on the pressure side trailing edge surface of the partitions. Service experience has demonstrated that the use of a protective coating alone will only provide about one to two years of SPE reduction when applied to conventional control stage nozzle designs. Thus the limited life of the available coating only produces a “time delay” in the erosion process. This limitation was recently overcome by the development of a new steam path design that significantly improves the erosion resistance of control stage nozzles. The new design (shown in Figure 39) uses slanted nozzle partitions which significantly reduce the number of particle impacts on the nozzle trailing edge pressure surface. Those impacts that do occur are at a reduced velocity and extremely shallow impact angles. A significant reduction in the rate of SPE damage is therefore obtained. The combination of this new nozzle shape with a protective diffusion coating produces a control stage nozzle design with three times the service life of conventional designs. This new design has been achieved with no sacrifice in the “as new” performance while providing tremendous benefits in long-term sustained efficiency. The heat rate benefit achievable is shown in Figure 40 for a typical unit on a five-year maintenance interval.

The SPE-resistant control stage design has become standard equipment on new units and can be accommodated in either a plate or nozzle box control stage design. It is retrofittable to existing nozzle box designs as well. Retrofitting a

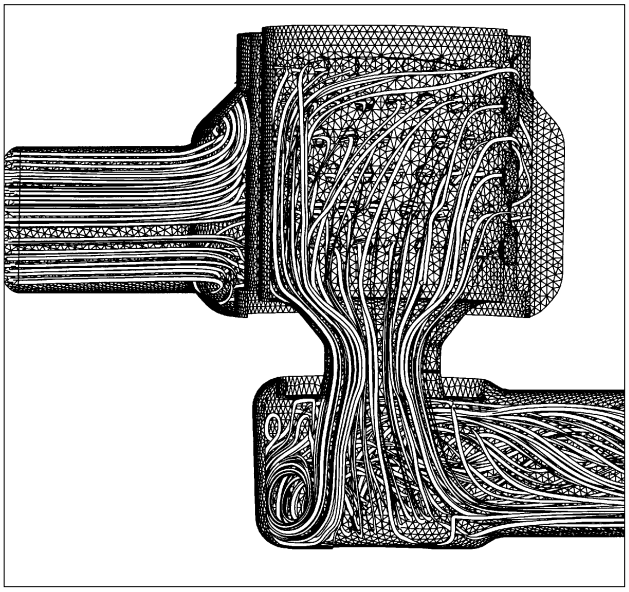

GT25811

Figure 38. NOVAK3D analysis of control valve

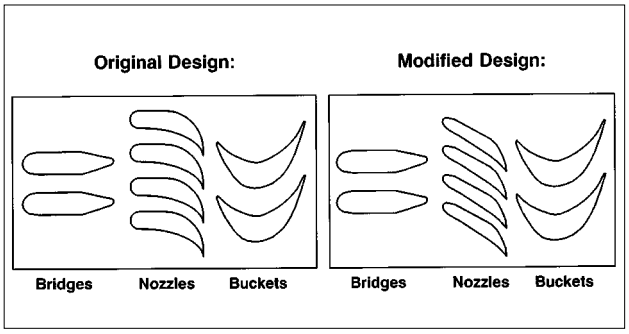

GT22201

Figure 39. Modified control stage to minimize SPE damage

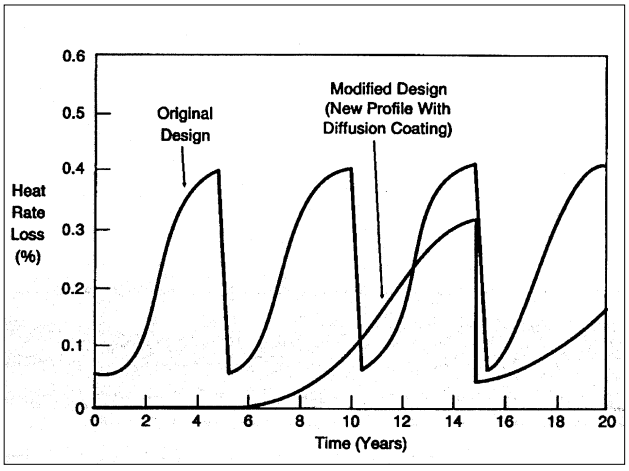

GT16903A

Figure 40. Control stage heat rate loss due to severe SPE damage

new SPE-design steam path restores the control stage efficiency to the "as new" level eliminating any nozzle profile losses that may have been caused from weld repairing eroded nozzles.

The new SPE-resistant control stage nozzle design has been in service since 1987. The initial application was made to two 650-MW supercritical double-reheat units with well-established histories of severe control stage SPE. In fact, the erosion was severe enough to require major control stage nozzle repairs on an 18- to 24-month cycle throughout the 1980s. The SPE design was run for three years (twice the normal time) before it was inspected in October 1990 during a planned maintenance outage. Figure 41 shows a side-by-side comparison of the condition of the new design after three years of service with the severely eroded conventional design after only one and a half years of service. The SPE design is virtually erosion-free. The utility demonstrated a 0.4% heat rate improvement after the first two years of service with the new design. They reinstalled the nozzle box with no repairs required and have extended the date of the next planned maintenance inspection based on the performance of the new SPE design.

Additional field confirmation of the SPE design has been obtained on two supercritical units with well-established histories of severe SPE. A major repair of the control stage nozzle was traditionally required on these machines every four to five years. The new SPE-resistant design was run for four years in one machine and four and a half in the other. Both machines were recently opened for inspection revealing only minimal SPE damage. No repairs were required and the nozzle boxes were returned to service.

Particle trajectory analysis has also been used to determine the cause of erosion to the first reheat stage nozzles and buckets. (For a detailed review of the analysis and its findings, see Reference 18.) The basic erosion mechanism at work in a reheat stage is a complex particle entrapment phenomena that results in the multiple rebounding of captured particles between the nozzles and buckets. As Figure 42 shows, the trajectory analysis demonstrated that first reheat-stage nozzle partition erosion results from the rebounding of particles from the leading edges of the buckets to the suction-side trailing edge region of the nozzles. The high tangential velocity acquired by the particles from their impact with the rotating buckets basically becomes the impact velocity of the particles as they strike the nozzle convex surfaces at a low

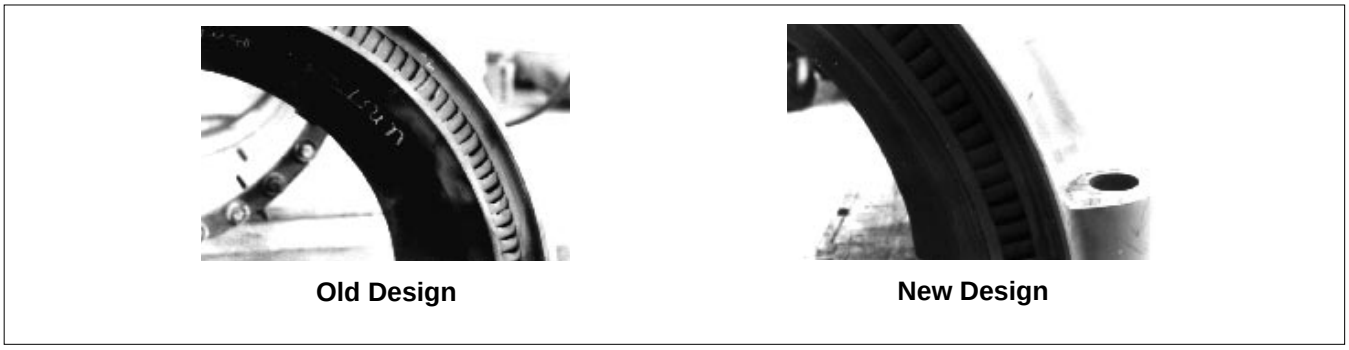

GT23105A

Figure 41. Field performance of new SPE resistant design

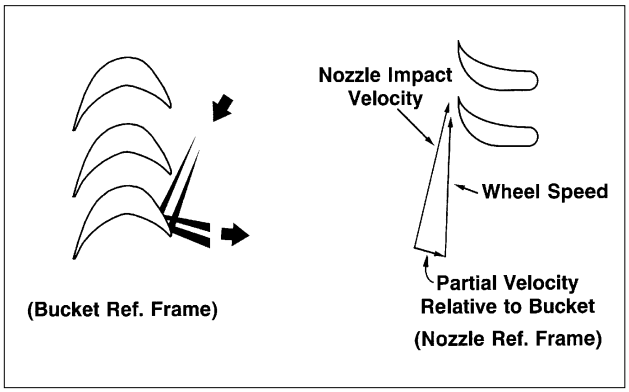

GT21959/GT22203

Figure 42. First reheat stage suction surface damage caused by particle rebounding

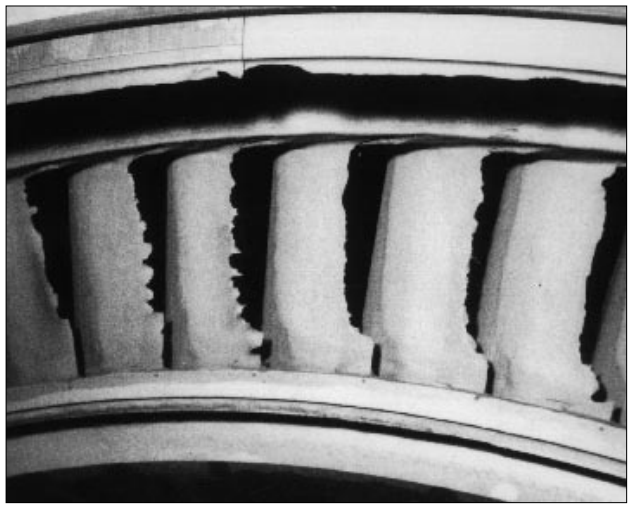

GT17232

Figure 43. Severe erosion on suction side of first reheat stage diaphragm

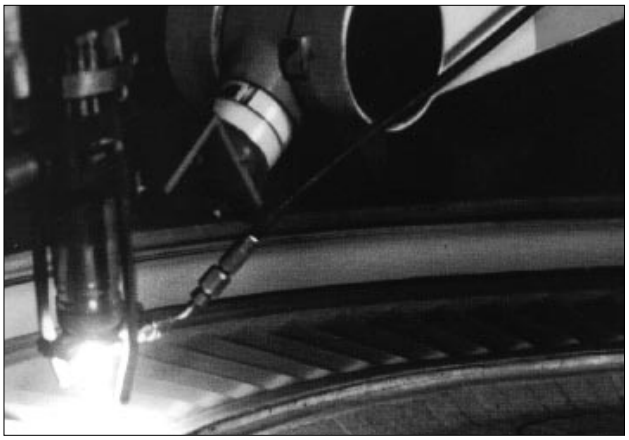

GT17231

Figure 44. Automated process coats reheat diaphragm

impact angle — a very erosive condition for the nozzles. Figure 43 shows the typical SPE damage experienced by a reheat diaphragm with the nozzle convex surface damage clearly evident.

As discussed in Reference 18, the most beneficial action that can be taken to combat the reheat erosion mechanism is to substantially increase the edge-to-edge axial clearance between the nozzles and buckets. Increasing this clearance profoundly affects the particle entrapment/rebounding mechanism to the point where the rebounding is nearly eliminated. Since some rebounding by very large particles may still persist even with an increased clearance, the nozzle trailing edge suction surface and the diaphragm outer sidewall are also protected by GE's newly developed Diamond Tuff™ HVOF (high velocity oxygen fuel) erosion-resistant coating. Figure 44 shows the coating being applied to a reheat diaphragm by a robot. (A more detailed description of the Diamond Tuff coating can be found in Reference 19.)

Figure 45 compares the performance deterioration produced by SPE of a conventional

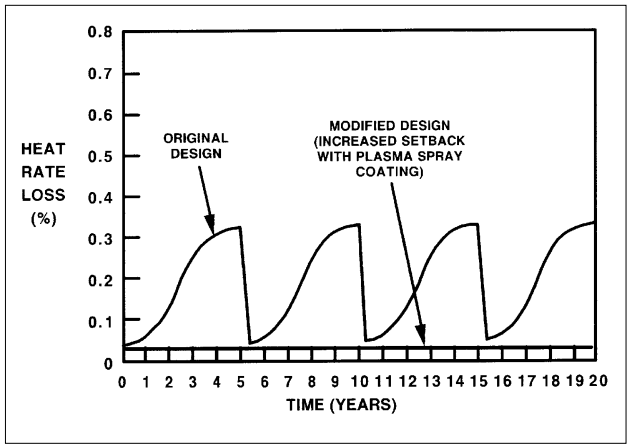

GT16904

Figure 45. First reheat stage heat rate loss due to severe SPE damage

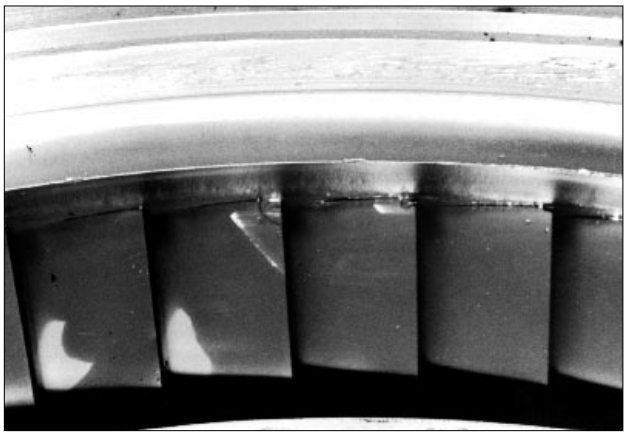

GT22204

Figure 46. SPE-resistant diaphragm after 3 1/2 years of service in the first reheat stage of a supercritical reheat turbine

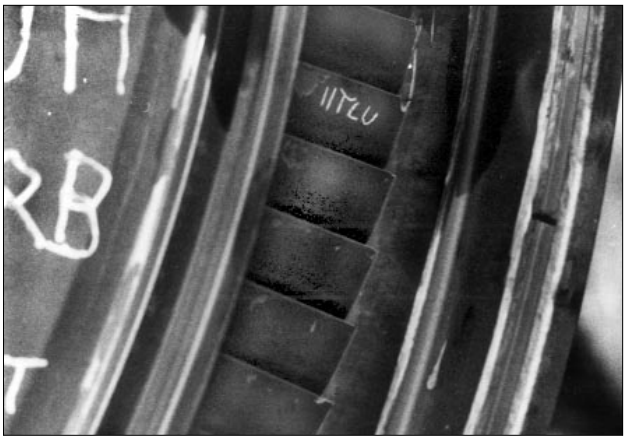

GT22205

Figure 47. SPE-resistant diaphragm after 3 1/2 years of service in the first stage of second reheat stage of a supercritical reheat turbine

reheat stage design with that expected from GE's new SPE-resistant design. A significant heat rate benefit is provided by the sustained efficiency available from the new design.

The new SPE-resistant design features have been incorporated into GE's new unit designs since 1985. They can also be retrofitted to a large selection of existing reheat diaphragm designs in service today, and many applications have been implemented since 1985. Figure 46 shows an SPE-resistant diaphragm that was in service for three and a half years in the first reheat stage of a super-critical reheat machine. The normal condition of the conventional first reheat stage diaphragm from that unit after three to four years of service was comparable to that shown in Figure 43. Negligible damage has occurred on the new design after the same time period. No repairs were required and the component was reinstalled in the unit.

The results of a more demanding application are shown in Figure 47. This diaphragm was installed in the first stage of the second reheat section of a super-critical double reheat machine with a previously demonstrated severe case of SPE. The relatively low design pressure of this stage aggravates the rebounding damage mechanism, providing a potent challenge for any SPE-resistant design. After three and a half years of service, Figure 47 shows the design to be up to the challenge. It was reinstalled in the unit without repairs to run until the next scheduled maintenance outage.

Positive Pressure Variable Clearance Packing

A recent innovation that improves the clearance control at shaft packings is the GE positive pressure variable clearance packing. Labyrinth seal packings close to the midspan of a high-temperature steam turbine rotor are susceptible to rubbing. Operation below the first critical rotor speed, acceleration through critical speeds, and boiler temperature variations all occur at startup, making the packing most vulnerable during this period. Excess clearance caused by rubbing during the startup of the unit results in increased fuel costs and a reduction in unit capacity. In addition, vibration problems associated with packing rubs can prevent the turbine from getting through its critical speeds, prolonging the startup of the unit. GE positive pressure variable clearance packing provides a large clearance during startup, and reduced clearance after the unit has synchronized. This

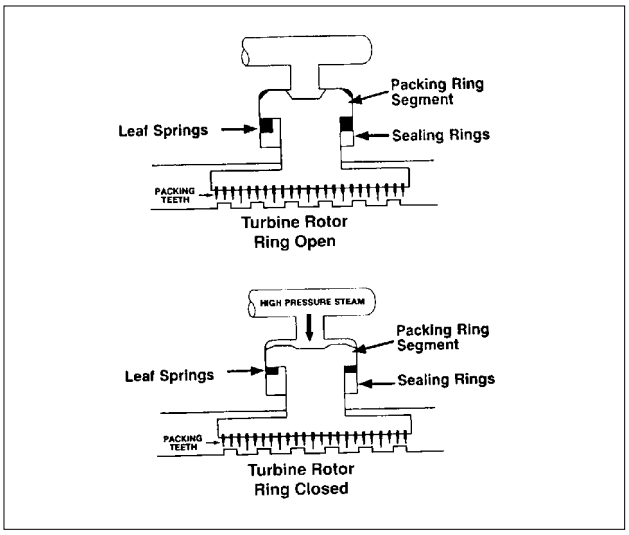

GT22026

Figure 48. GE positive pressure packing

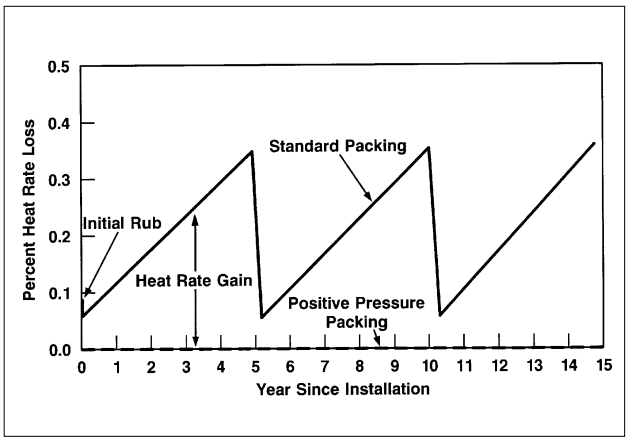

GT22207

Figure 49. Heat rate improvement for positive pressure packing in 500 MW units

arrangement minimizes rubs associated with turbine startups while providing optimum sealing when the unit is loaded.

The GE positive pressure variable clearance packing, shown in Figure 48, utilizes a combination of the pressure drop across the packing and an additional pressure force, when required, to close the packing rings after synchronization. Also, an external control of the packing rings in a mid-span packing of an opposed flow unit can be provided. This allows the unit to be prewarmed by pressurization on turning gear after a prolonged outage without the unit rolling off turning gear. A more detailed description of the positive pressure variable clearance packing is given in Reference 20.

For an example of the application of positive pressure packing, consider a 500 MW reheat unit that has opposed-flow HP and IP sections in a single casing. The internal mid-span packing (N2 packing) and the first three HP and IP stage diaphragm packings are susceptible to rubs during the startup of the unit. The normal design clearance for these packings is 0.015 inch (0.381 mm), but after five years of operation, the packing clearance is typically found to be opened up to 0.06 inch (1.524 mm). The impact of this increased radial packing clearance on heat rate can be calculated using Reference 21. Compared to design, the 0.06 inch (1.524 mm) radial clearance causes the unit to experience a heat-rate loss of about 0.35%. The packings are normally replaced every five years and the clearances restored. Figure 49 shows this performance loss with time for the present standard packings, assuming that the clearance increases linearly with time. Application of the positive pressure packings will eliminate the major shaft packing rubs since these rubs usually occur at startup, when the positive pressure shaft packings have a large radial clearance. The positive pressure packings will hold design clearance with time, since they will not be subject to the startup transients seen by the standard packings. Therefore, the heat rate advantage of the positive pressure packing would be the area under the curve shown on Figure 49.

In another example, positive pressure variable clearance packings were installed on the internal packing between the HP and IP sections (N2 packing) and the first three HP and IP stages of the 525 MW Jim Bridger #2 unit of Pacific Power & Light. Although no efficiency tests were conducted to identify the improvement resulting from the HP and IP diaphragm packings, pressure measurements were recorded at the startup of the unit that clearly demonstrated the closure of each of the packing rings in the N2 packing. Similar tests were conducted after six months of operation that demonstrated the continued successful operation of the positive pressure packings.

Typical economic payback periods for installing positive pressure variable clearance packing have been less than a year.

LABORATORY TEST PROGRAMS

Subsonic Air Turbine

The principal test vehicle used for the development of new stage design concepts is the subsonic air turbine located in GE Power

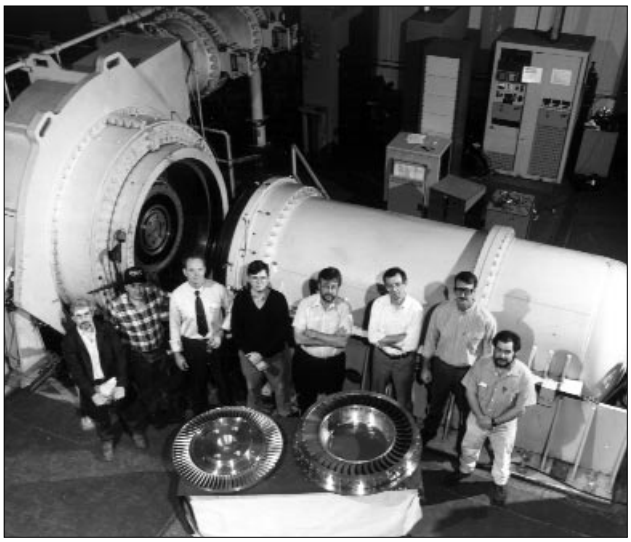

GT24585

Figure 50. Subsonic air turbine test facility

Generation's Aerodynamic Development Laboratory in Schenectady, New York. This rig, shown in Figures 50 and 51, permits the quick and accurate evaluation of turbine test stages at actual operating speeds and pressure ratios using compressed air as the working fluid. In addition to traditional performance testing, nozzle and stage exit traversing as well as laser-assisted data acquisition procedures are employed to collect more detailed flow field information. Numerous new configurations have been tested in this facility over the past several years to confirm that significant efficiency gains have been achieved, and to validate the CFD codes.

The facility is arranged as a closed loop. A 4810 HP centrifugal compressor is used to circulate the air around the loop and a smaller make-up air compressor permits the desired stage inlet pressure to be maintained. Prior to reaching the test section, the air supply passes through a water-cooled heat exchanger to permit the stage inlet temperature to be accurately maintained. A hydraulic actuation system slides the inlet plenum apart from the exhaust scroll, permitting easy access to the test stage. Test wheels are about 38 inches (965 mm) in diameter overall and have active blade lengths in the 2-inch (50.8 mm) to 5-inch (127 mm) range. Shaft speeds vary between 2000 and 4800 RPM. A typical intermediate-pressure test stage produces about 650 HP (485 kW) near its design point. Figure 52 shows a typical air turbine test diaphragm with compound lean nozzles designed for an intermediate pressure stage, while Figure 53 shows the test wheel for the same stage.

A water-cooled inductor type dynamometer that is supported on hydrostatic oil pads is used to measure the shaft torque developed by the wheel. An enhanced accuracy rotary torque meter provides an additional torque reading for comparison and redundancy. A coupling that

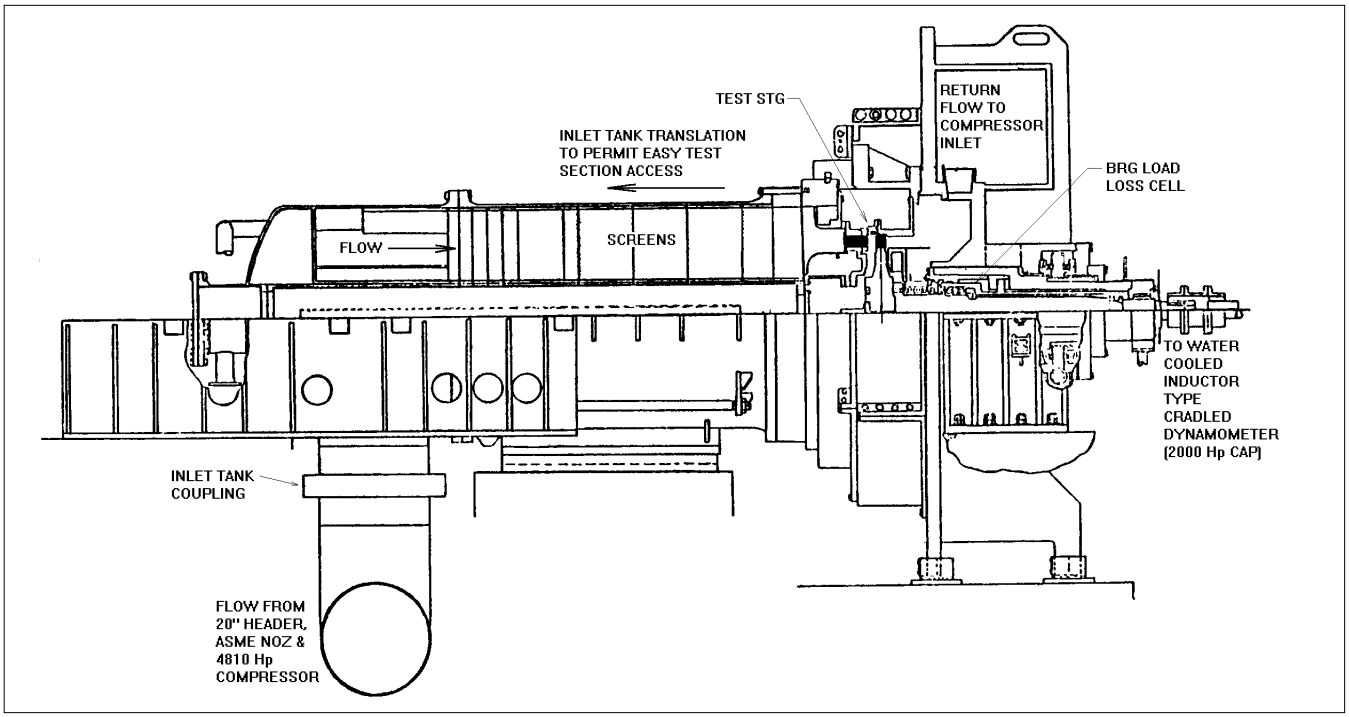

GT25805

Figure 51. Cross-section of subsonic air turbine test facility

RDC27193-03-06

Figure 52. Advanced Vortex test diaphragm

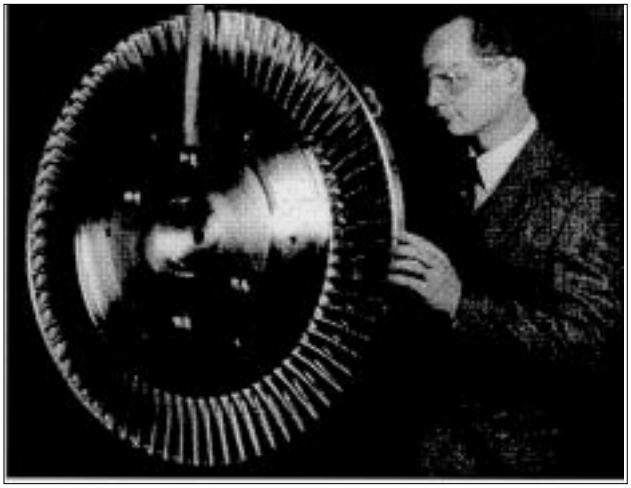

RDC27193-03-06

Figure 53. Advanced Vortex "blisk" test wheel

permits axial movement is used for the gear-driven positioning of the wheel relative to the diaphragm. This feature is particularly useful for accurately setting the nozzle-to-bucket axial gap and it provides a way to easily study the effect of changing the edge-to-edge distance. A bearing load loss cell system floats the entire stub shaft and bearing assembly on a hydrostatic oil film. This permits the torque loss due to bearing friction to be accurately determined during all running conditions.

Traversing at nozzle and bucket exit planes is done using thermocouple probes for temperature measurement, and three-hole wedge and

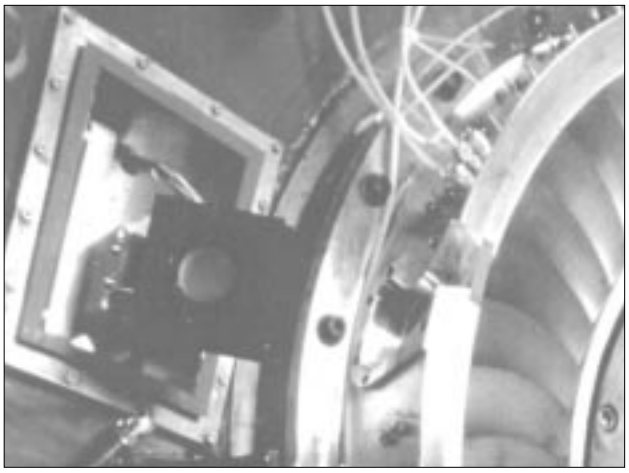

GT25812

Figure 54. Laser tunnel and optics in subsonic air turbine

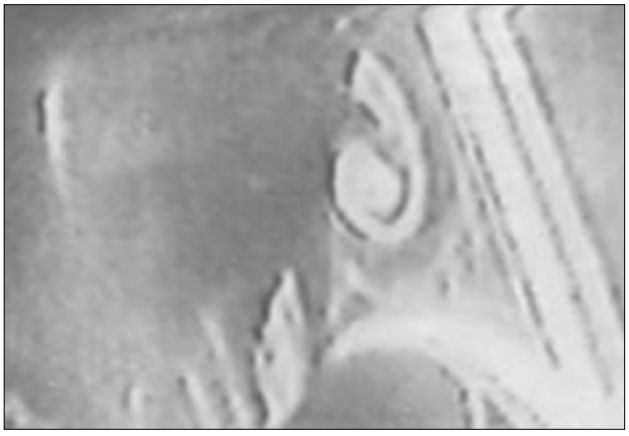

GT25806

Figure 55. Laser light plane flow visualization

cobra probes with auto-nulling features for pressure and flow angle measurements. A recent innovation in the facility allows laser Doppler velocimetry and laser light plane flow visualization techniques to be used to further GE's knowledge of the flow mechanisms responsible for improved stage designs. An instrumentation tunnel that includes a five-axis traverse mechanism (shown in Figure 54) permits the accurate positioning of laser probes and a mirror for directing the laser light into the interior of a nozzle passage. The laser light passes through a specially designed fused silica window installed in the outer wall of the diaphragm. Figure 55 shows a vortex structure at the exit plane of a leaned nozzle visualized with the laser light plane technique. The laser light plane data acquisition system is currently undergoing development to improve its ability to capture video images of flow features with greater clarity. This technique, along with the laser Doppler

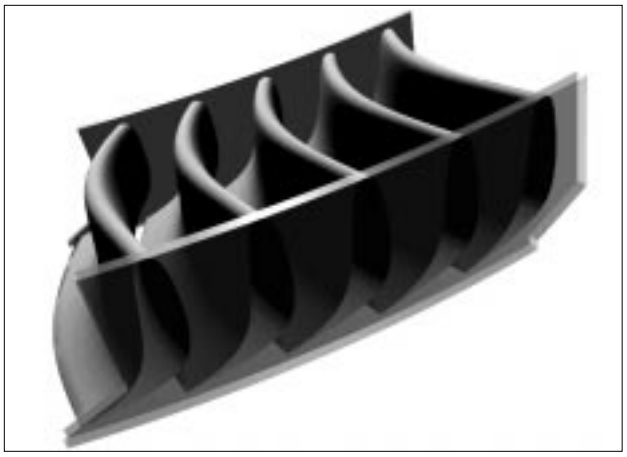

GT25783

Figure 56. Computer-generated model of Advanced Vortex diaphragm segment

GT25807

Figure 57. Tip seal test rig

velocimetry, is providing additional data for validating the CFD codes used to design and evaluate alternative aerodynamic design concepts.

Air turbine test wheels, such as the one shown in Figure 53, are produced as a “blisk” (short for “bladed disk”). The wheel, buckets and integral bucket covers are machined out of a single disk of metal with a high degree of precision using state-of-the-art five-axis NC machining technology. The blisk construction eliminates the time-consuming operations associated with assembling individual buckets on the wheels, and reduces the manufacturing time by more than 50%. Before a new design concept is committed to test hardware, a computer-generated model is created, such as the one shown in Figure 56 for a diaphragm segment with compound lean nozzles. Full size plastic parts are made from the computer-generated model using a stereolithography process to visualize the new components, and to perform manufacturing producibility studies. By using these rapid prototyping methods, we have dramatically reduced our development cycle time for new aerodynamic design concepts, and have accelerated the introduction of new high efficiency features into our product line.

Tip Seal Test Rig

New non-contacting leakage control devices are tested in the rig shown in Figure 57 using compressed air. The rig accommodates stationary two-dimensional models of seal geometries that are machined into six-inch long (152 mm) flat plates. These seal strips feature straight, slant, stepped, high-low and other tooth arrangements in combination with smooth and contoured bucket cover or shaft surfaces. For bucket tip seal tests, the test section in the rig can simulate the leakage flow that goes over the bucket cover and through the bucket tip seal, as well as the main flow that goes under the cover and contributes to the stage output. These flows are kept separate and can be independently controlled and measured. The leakage flow is measured using an ASME orifice plate, while the main flow is measured using an ASME flow nozzle. The pressure level in the main flow and the pressure ratio across the seal can also be varied separately. The maximum pressure ratio that can be achieved across the seal is 2.5.

CFD analyses are used along with this rig to screen potential seal design candidates. Figure 23 shows typical data obtained in the rig in a recent test series designed to determine the optimum tooth spacing for a slant tooth bucket tip seal, while Figure 25 shows the equivalent CFD analysis. The more promising candidates are then tested on a running stage in the air turbine.

GEAE Low Speed Research Turbine

Test facilities at the GE Aircraft Engines Aerodynamics Research Laboratory in Cincinnati, Ohio, are also used to develop new aerodynamic design concepts for steam turbines. The large-scale, multi-stage low speed research turbine (LSRT) shown in Figure 58 is used to test large-scale models containing up to three stages in an environment where very detailed measurements of the flowfield can be made. A cross-section of the LSRT is shown in Figure 59. The LSRT has a constant casing diameter of 60 inches (1.524 m), a vertical axis of rotation, a calibrated intake system, and Plexiglas casing windows which mount into large steel casings. Ambient air is pulled through the

GT24586

Figure 58. Low speed research turbine test facility at GE Aircraft engines

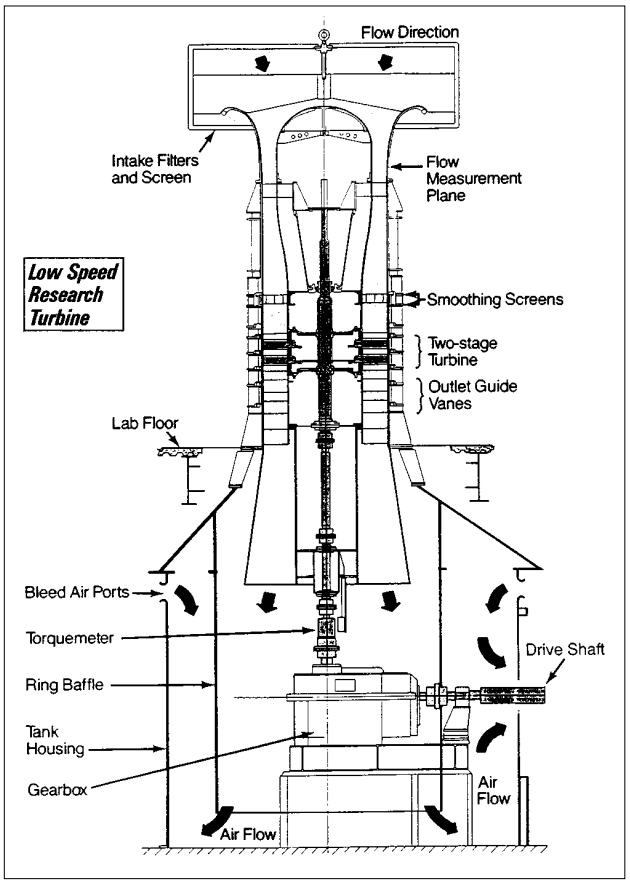

GT25800

Figure 59. Cross-section of low speed research turbine test facility

turbine blading from the inlet at the top into a large plenum beneath the turbine. This air, which is drawn through the blading by a large centrifugal blower located next to the plenum, causes the turbine to rotate. The power generated by the test turbine is used to assist in driving the blower, saving roughly one-third of the power requirements for the facility. The design tip speed for the turbine is 161 ft/sec (49.1 m/sec) at 616 RPM.

The rate of mass flow through the turbine is controlled by a set of variable inlet guide vanes on the blower and by variable air-bleed valves in the outer cylinder. The blower exhausts the air from the turbine into an air-handling/mixing system outside the laboratory. This system mixes the exhaust air with outside ambient air in varying proportions before it is returned to the lab building, thereby maintaining a constant temperature and pressure environment in the lab.

Individual nozzles and buckets are precision-molded from high-strength plastic and assembled into rings and discs, thus allowing a wide variety of turbine geometries to be modeled. The airfoils are large enough to be instrumented with a matrix of static pressure taps. A rotating scanivalve and slipring allow measurements to be made in the rotating frame. A variety of measurement techniques, including laser Doppler velocimetry, are used to gather detailed information about the flowfield.

FIELD TEST PROGRAMS

GE recognizes that the true measure of the performance of a new design feature is its performance in the field. Analytical predictions and laboratory tests are extremely valuable, but it is the field test that once and for all demonstrates the value and integrity of a new feature. Consequently, extensive precision field tests are performed on all of the new steam path design features described in this paper as they are introduced in actual operating units. To date, all units incorporating advanced aerodynamic design features that have been field tested have met their performance guarantees. The data obtained from these tests is used to calibrate the CFD codes to ensure that these increasingly complex codes are firmly grounded in reality, and are giving the designers the right answers. As these CFD methods are validated by test data, the need for expensive prototype testing will

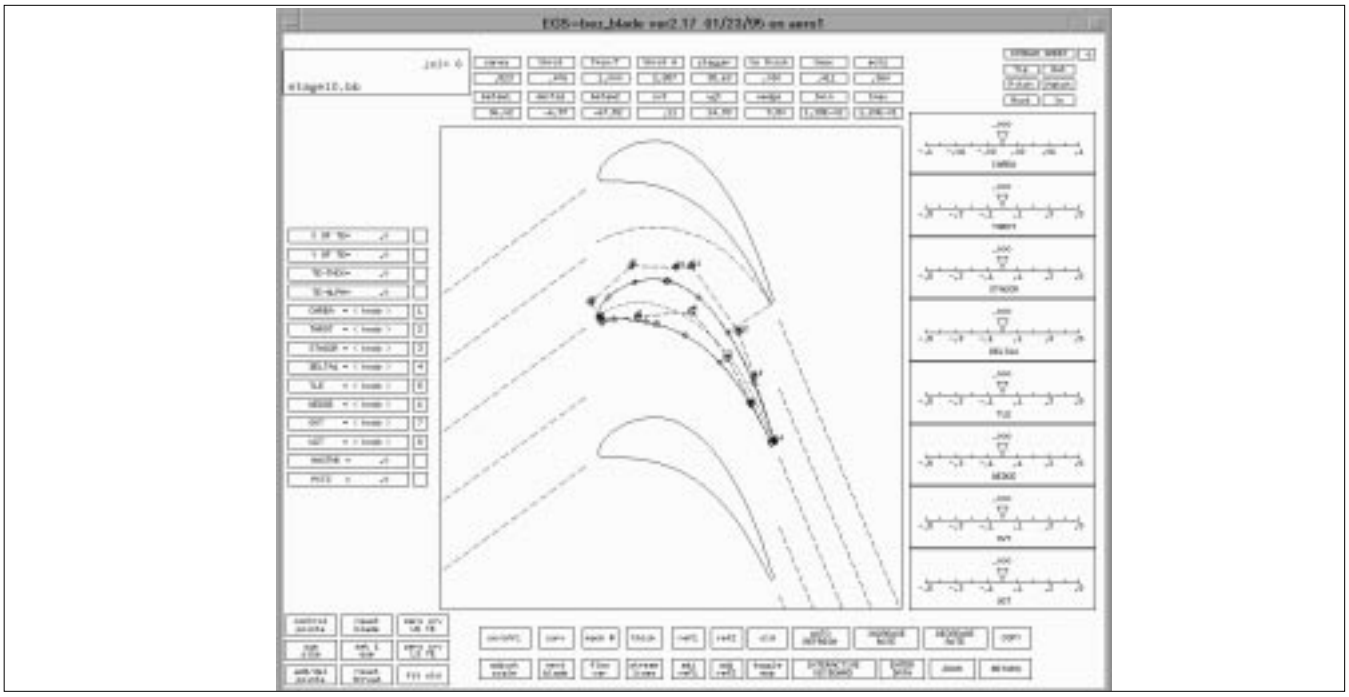

GT25808

Figure 60. Bezblade screen

diminish, leading to substantial reductions in development cycle time and cost and more efficient, reliable turbine designs.

DESIGN AUTOMATION AND OPTIMIZATION

For new turbine designs, it is often necessary to perform numerous labor-intensive and time-consuming design iterations before all design requirements are met. The turbine stages in a given section must be optimized to produce maximum efficiency, while at the same time numerous mechanical and producibility requirements must be met. To achieve dramatic reductions in design cycle time, GE has developed a suite of powerful computer-based steam path design automation and optimization tools.

CRD has developed a unique and innovative workstation-based tool for the design of blade cross-sections. In this tool, called Bezblade, blade cross-section shapes are described in parametric form as smooth Bezier curves. Through a user-friendly graphical interface, shown in Figure 60, the aerodynamic designer has direct control over familiar geometric design parameters such as blade stagger, passage throat, blade thickness, cross-section area, and leading and trailing edge wedge angles. The blade shape can be changed by either using a mouse to drag the Bezier curve control points, by dragging sliding controls representing each design parameter, or by directly typing in the parameter values. The Bezier curve representation allows individual parameters to be varied without requiring fine tuning of the other parameters to achieve reasonable shapes. The program is coupled to a fast 2D flow solver that allows the designer to manipulate the blade shape and receive quick feedback on the effect of the shape change on the blade surface Mach number distribution. Individual blade cross-sections can be radially stacked to form a complete blade, and curves

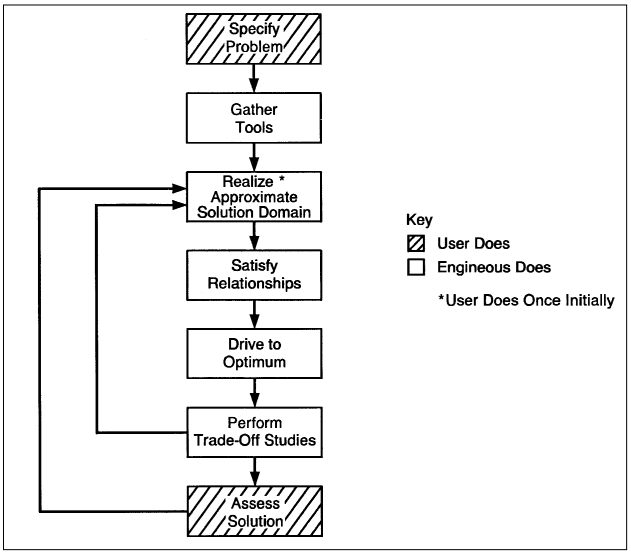

GT22214B

Figure 61. Engineous design optimization process

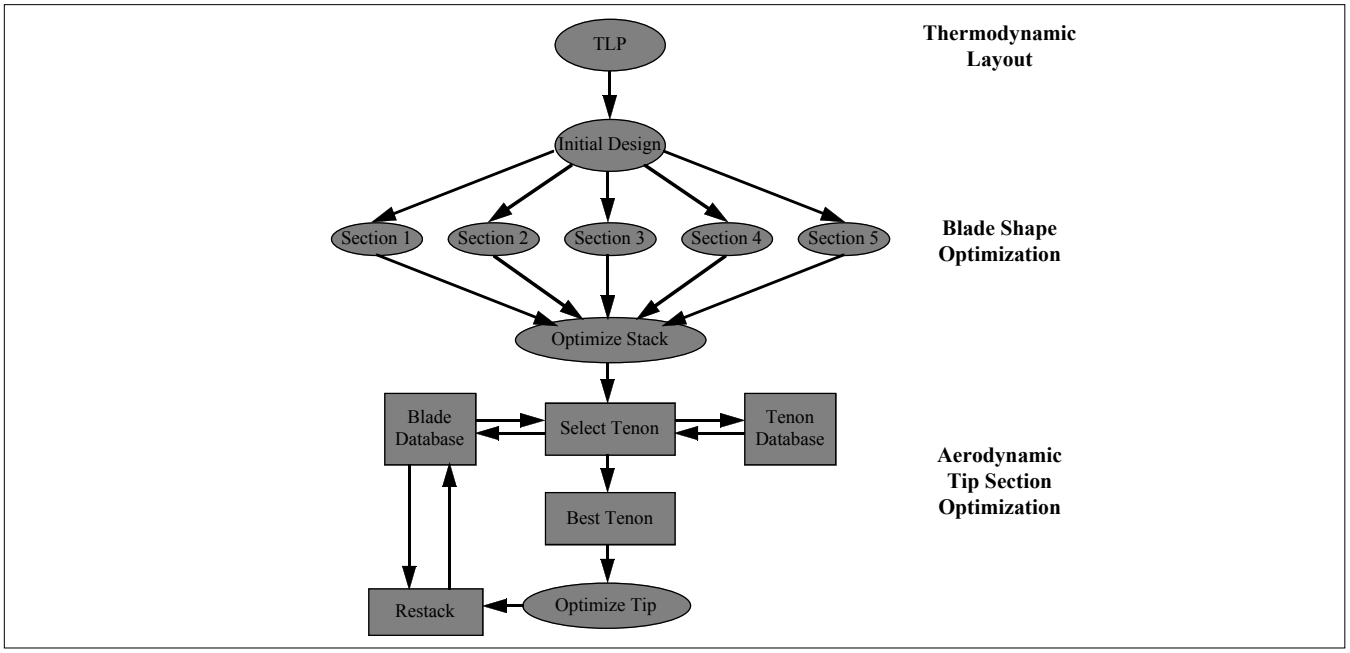

Figure 62. TLP/TADS blade design optimization process

are automatically plotted of the various blade geometry parameters as functions of radius. By directly modifying these curves using the mouse, the stackup can be quickly smoothed out to produce the final blade shape.

A significant improvement was made to Bezblade by coupling it to a 2D version of NOVAK3D and using a linear perturbation method to compute sensitivities of the flow solution to the positions of each of the Bezier control points. Once the sensitivities have been computed, the designer can manipulate the blade shape and receive immediate, real-time updates on the effect of the shape change. The blade surface Mach number distribution changes literally as fast as the designer can change the shape with his mouse.

Bezblade has been used with great success to design advanced vortex stages for production units. While this design tool has dramatically reduced design cycle time, the design engineer must still use Bezblade in a manual, iterative fashion until he is satisfied that he has achieved an optimum design, and he must visually evaluate the quality of the blade design. To achieve further reductions in cycle time in the optimization process, GE has made use of a design optimization computer program developed by CRD, called Engineous (References 22 and 23). As shown in Figure 61, Engineous is a user-friendly generic software shell that automatically iterates design programs until constraints and design goals are met. It captures human design knowledge in a "knowledge base" by querying the engineer for the required rules. It does not attempt to replace the designer, but retains the knowledge of different specialists in multiple disciplines. When the design knowledge is incomplete, which is often the case with rapidly changing technology or very large knowledge domains, Engineous combines its own intelligent searching heuristics with the existing knowledge to solve the problem. It performs the tedious work required to iterate design and analysis codes, such as manipulating and editing input data, running programs, scanning output files, and it applies design knowledge to modify design parameters. By delegating this work to Engineous, engineers can realize a 10:1 improvement in the time required to develop a new design, can minimize human error and can achieve improved designs.

Because Engineous is automated, it can explore many more design options and parameter trade-offs in a given period of time. Additionally, the program's own searching heuristics and numerical optimization techniques often turn up new design solutions that designers had not thought of before. Engineous can also couple design codes from many disciplines, such as aerodynamics and mechanical design, to effectively balance interrelated and often conflicting goals. The program dynamically displays its results as they unfold, allowing designers to analyze solutions during and after the run, applying their own judgment to the

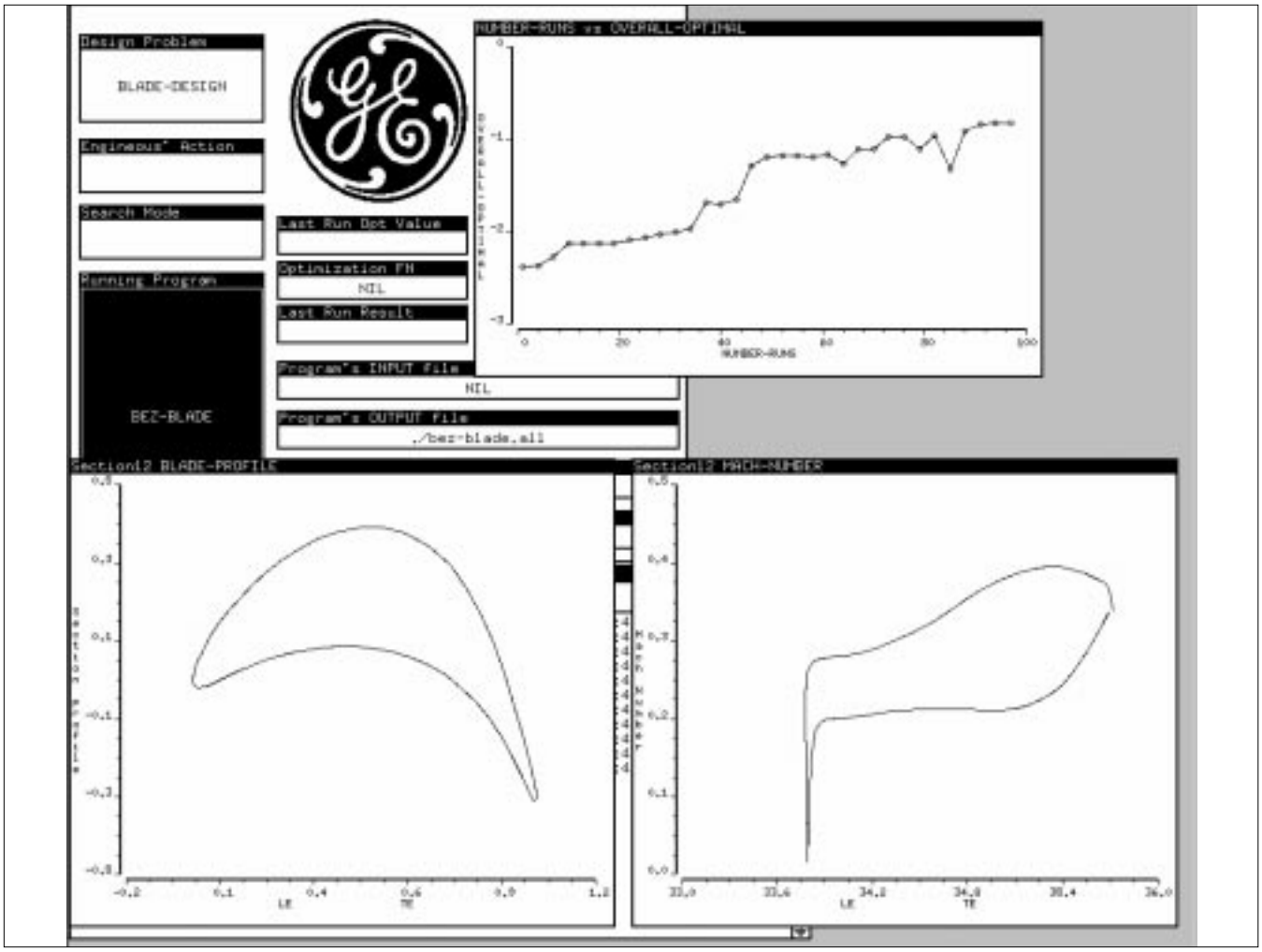

GT25810

Figure 63. TADS/Engineous screen

problem. The program has been used successfully by many GE components for the design of such products as aircraft engine centrifugal compressors and turbines, superconducting generators, cooling fans, and DC motors. GE Power Generation is also using it to optimize power plant cycles.

GE Aircraft Engines has used Engineous for preliminary turbine stage layout (References 24 and 25) and achieved a better than five to one improvement in design cycle time. Encouraged by this success, GE Power Generation coupled a quasi-3D throughflow program to Engineous, so that the radial flow distribution in advanced vortex stages could be optimized. Engineous automatically runs a sequence of six design codes to optimize the radial flow distribution for a given stage in only a few hours running on a workstation, a procedure that used to take an engineer several weeks to do manually.

Based on the success of an early attempt by GEAE to use Engineous to design airfoil sections (Reference 26), GE Power Generation and CRD developed an automated workstation-based system that uses Engineous to optimize three-dimensional blade profiles to maximize efficiency while meeting all mechanical design requirements. The system was created by coupling Engineous to Bezblade, a 2D flow solver, a knowledge base containing aerodynamic and mechanical design rules and constraints, and a number of other blade design utilities. This suite of programs is known as the Turbine Airfoil Design System (TADS), and it is described in Reference 27.

The overall blade design process is illustrated in Figure 62. The initial layout of the turbine section is done by the Thermodynamic Layout Program (TLP) module, which generates thermodynamic data including entrance and exit flow angles for all of the blade rows based on a quasi-3D streamline calculation. This layout incorporates the effect of blade lean and other advanced vortex features. An engineer sets up

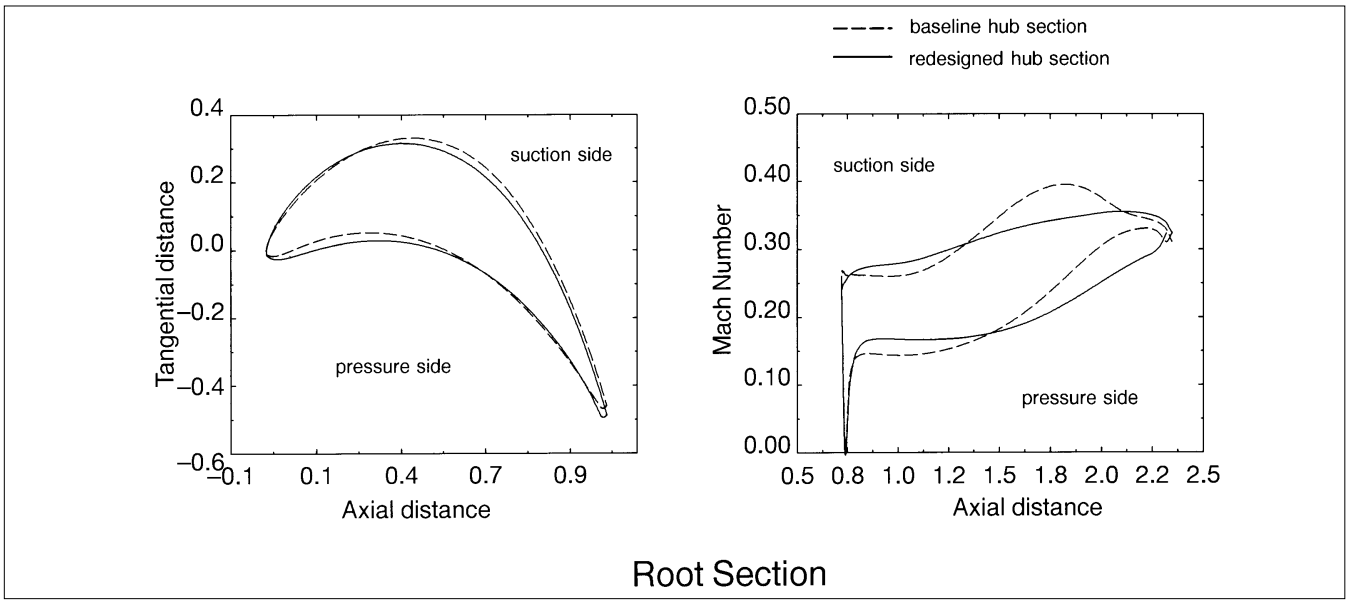

Figure 64. Results of TADS blade shape optimization

Figure 65. Solid model of typical bucket designed by TADS

an initial baseline blade design file based on TLP output, and launches TADS. For each bucket design, five cross-sections equally spaced from root to tip are designed simultaneously on five separate workstations to reduce the design cycle time. For each of these cross-sections, Engineous changes the blade cross-section shape using Bezblade, runs the flow solver, evaluates the output and makes new changes to the shape based on the results of its last change. It continues to iterate on the design until it achieves maximum blade "quality," which is defined as a combination of factors that ensure that the optimum blade surface Mach number distribution is achieved, and that the blade shape is radially smooth. The most difficult element in the system to develop was the translation of the designer's visual subjective perception of the design into an analytic evaluation that the computer could perform.

The designer can monitor the optimization process for each cross-section by calling up the workstation screen shown in Figure 63. The current blade shape is displayed in the lower left window, and the corresponding blade surface Mach number plot is displayed in the lower right window. The blade quality parameter is displayed in the upper right window. Figure 64 illustrates the type of shape changes made by the system during the optimization process. These windows are updated every few seconds as the optimization proceeds. Typical cross-section designs require one to four hours of execution time, depending on the quality of the initial baseline design.

Once the five cross-sections have been designed, TADS brings them together and uses Engineous to smooth out the blade stackup. The system then enters the tenon database and selects a tenon that meets mechanical design requirements and fits on the bucket tip section as closely as possible. If the tenon cross-section is larger than the vane tip section, Engineous redesigns the tip section to fit around the tenon, and then modifies the vane below the tip section

to achieve a smooth blend. Figure 65 shows a typical intermediate-pressure bucket designed by the system.

This system is now used to design all advanced vortex buckets for production steam turbines. It is also being used to design airfoils for aircraft engines and advanced gas turbines. A fifteen-to-one reduction in design cycle time has already been achieved, and further gains continue to be made as the system is refined. By incorporating mechanical design constraints into the system, TADS allows us to design fully customized turbines that exactly meet the needs of each individual customer in considerably less time than it took in the recent past, and with no compromise in mechanical integrity and reliability. This remarkable design tool also allows us to respond to retrofit opportunities more quickly, thus giving our customers more options for improving existing designs.

CONCLUSION

In this paper, recent advances in GE steam path technology have been described. Advanced computational fluid dynamics codes are being used to develop new aerodynamic design concepts to dramatically improve efficiency. Extensive laboratory test programs are being performed to verify the predicted efficiency gains of new design features, and to validate the CFD codes. Unique design automation and optimization tools have been developed that allow fully customized and cost-effective turbines to be designed in short cycle times to meet the needs of individual customers.

REFERENCES

1. Langston, L.S., "Crossflows in a Turbine Cascade Passage," ASME Journal of Engineering for Power, Vol. 102, No. 4, October, 1980, pp. 866-874.
2. Holmes, D.G. and Tong, S.S., "A Three-Dimensional Euler Solver for Turbomachinery Blade Rows," ASME Journal of Engineering for Gas Turbines and Power, Vol. 107, April, 1985, pp. 258-264.
3. Turner, M.G. and Jennions, I.K., "An Investigation of Turbulence Modeling in Transonic Fans Including a Novel Implementation of an Implicit k-e Turbulence Model," ASME Paper 92-GT-308, 1992.
4. Turner, M.G., Liang, T., Beauchamp, P.P. and Jennions, I.K., "The Use of Orthogonal Grids in Turbine CFD Computations," ASME Paper 93-GT-38, 1993.
5. Holmes, D.G. and Warren, R.E., "Detailed Studies of Inviscid Secondary Flows," GE CRD Report No. 85CRD133, July, 1985. Presented at the 1985 ASME Winter Annual Meeting, 11/18/85.
6. Connell, S.D., Holmes, D.G. and Braaten, M.E., "Adaptive Unstructured 2D Navier-Stokes Solutions on Mixed Quadrilateral/Triangular Meshes," ASME Paper 93-GT-99, 1993.
7. Connell, S.D. and Holmes, D.G., "A 3D Unstructured Adaptive Multigrid Scheme for the Euler Equations," AIAA Paper 93-3339, 1993.
8. Braaten, M.E. and Connell, S.D., "A 3D Unstructured Adaptive Multigrid Scheme for the Navier-Stokes Equations," GE CRD Report No. 94CRD146, August, 1994.
9. Rai, M. and Madavan, N., "Multi-Airfoil Navier-Stokes Simulations of Turbine Rotor-Stator Interaction," Journal of Turbomachinery, Vol. 112, July, 1990, pp. 377-384.
10. Adamczyk, J.J., Celestino, M.L., Beach, T.A. and Barnett, M., "Simulation of Three-Dimensional Viscous Flow Within a Multistage Turbine," ASME Paper 89-GT-152, 1989.
11. Dejch, M.E., et al., "Method of Raising the Efficiency of Turbine Stages with Short Blades," Teploenergetika, February, 1960, pp. 18-24.
12. O'Connor, M.F., Robbins, K.E. and Williams, J.C., "Redesigned 26-Inch Last Stage for Improved Turbine Reliability and Efficiency," ASME Paper No. 84-JPGC-GT-17, 1984. (Also published as GE Power Generation Turbine Technology Reference Library Paper No. GER-3399, 1984.)
13. O'Connor, M.F., Williams, J.C., Dinh, C.V., Ruggles, S.G. and Kellyhouse, W.W., "An Update on Steam Turbine Redesigns for Improved Efficiency and Availability," GE Power Generation Turbine Technology Reference Library Paper No. GER-3577, 1988.
14. Morson, A., "Steam Turbine Long Bucket Developments," GE Power Generation Turbine Technology Reference Library Paper GER-3647, 1990.
15. Morson, A.M., Williams, J.C., Pedersen, J.R. and Ruggles, S.G., "Continuously Coupled 40-Inch Titanium Last Stage Bucket Development," GE Power Generation

Turbine Technology Reference Library Paper No. GER-3590, 1988.
16. Moore, J.H., "High-Power-Density™ Steam Turbine Design Evolution," GE Power Generation Turbine Technology Reference Library Paper No. GER-3804, 1994.
17. Sovran, G. and Klomp, E.D., "Experimentally Determined Optimum Geometries for Rectilinear Diffusers with Rectangular, Conical or Annular Cross-Section," from Fluid Mechanics of Internal Flow, edited by G. Sovran, symposium held at General Motors Research Laboratories in Warren, MI in 1967, published by Elsevier Publishing Co.
18. Sumner, W.J., Vogan, J.H. and Lindinger, R.J., "Reducing Solid Particle Damage in Large Steam Turbines," Proceedings of the American Power Conference, Vol. 47, 1985, pp. 196-212. (Also published as GE Power Generation Turbine Technology Reference Library Paper No. GER-3478A, 1985.)
19. Shalvoy, R.S., et al, "An Improved Coating for the Protection of Steam Turbine Buckets from SPE," presented at the EPRI Steam Turbine/Generator Workshop, July 20-23, 1993, Albany, NY.
20. Morrison, B.L., Booth, J.A. and Schofield, P., "Positive Pressure Variable Clearance Packing," 1989 EPRI Heat Rate Improvement Conference, Knoxville, Tenn.
21. Schofield, P., "Maintaining Optimum Steam Turbine-Generator Thermal Performance," Missouri Valley Electric Association 1981 Engineering Conference, Kansas City, Mo.
22. Powell, D.J, Skolnick, M.M. and Tong, S.S., "Engineous: A Unified Approach to Design Optimization," Applications of Artificial Intelligence in Engineering, Vol. 1: Design, pp. 137-157, Computational Mechanics Publications, Southampton, UK, 1990.
23. Ashley, S., "Engineous Explores the Design Space," Mechanical Engineering, Vol. 114, No. 2, February 1992, pp. 49-52.
24. Lee, H., Goel, S. and Tong, S.S., "Toward Modeling the Concurrent Design of Aircraft Engine Turbines," ASME Paper 93-GT-193, 1993.
25. Goel, S., Gregory, B.A. and Cherry, D.G., "Knowledge-Based System for the Preliminary Aerodynamic Design of Aircraft Engine Turbines," Society of Photo-optical Instrumentation Engineers, Applications of Artificial Intelligence, Knowledge-Based Systems in Aerospace and Industry, April 13-15, 1993, Orlando, Florida.
26. Shelton, M.L., Gregory, B.A. and Lamson, S.H., "Optimization of a Transonic Turbine Airfoil Using Artificial Intelligence, CFD and Cascade Testing," ASME Paper 93-GT-161, 1993.
27. Goel, S., Singh, H. and Cofer, IV, J.I., "Turbine Airfoil Design Optimization," ASME Paper 96-GT-158, 1996, presented at the ASME Turbo Expo '96 conference in Birmingham, UK, June 11, 1996.

Note: Substantial portions of this paper appeared in ASME Paper 95-CTP-2, "Advances in Steam Path Technology," published in the Journal of Engineering for Gas Turbines and Power, Vol. 118, April 1996, pp. 337-352.

LIST OF FIGURES

For further information, contact your GE Field Sales Representative or write to GE Power Systems Marketing

GE Power Systems

General Electric Company
Building 2, Room 115B
One River Road
Schenectady, NY 12345

8/96